

# Ice thickness and bed topography of Jostedalsbreen ice cap, Norway

Mette K. Gillespie<sup>1</sup>, Liss M. Andreassen<sup>2</sup>, Matthias Huss<sup>3,4,5</sup>, Simon de Villiers<sup>1</sup>, Kamilla H. Sjurssen<sup>1</sup>, Jostein Aasen<sup>2</sup>, Jostein Bakke<sup>6</sup>, Jan M. Cederstrøm<sup>6</sup>, Hallgeir Elvehøy<sup>2</sup>, Bjarne Kjøllmoen<sup>2</sup>, Even Loe<sup>7</sup>, Marte Meland<sup>8</sup>, Kjetil Melvold<sup>2</sup>, Sigurd D. Nerhus<sup>1</sup>, Torgeir O. Røthe<sup>1</sup>, Eivind W. N. Støren<sup>6,9</sup>, Kåre Øst<sup>10</sup>, Jacob C. Yde<sup>1</sup>

<sup>1</sup>Department of Civil Engineering and Environmental Sciences, Western Norway University of Applied Sciences, Sogndal, 6851, Norway

<sup>2</sup>Section for Glaciers, Ice and Snow, Norwegian Water Resources and Energy Directorate (NVE), Oslo, 0301, Norway

<sup>3</sup>Laboratory of Hydraulics, Hydrology and Glaciology (VAW), ETH Zurich, Zurich, 8092, Switzerland

<sup>4</sup>Swiss Federal Institute for Forest, Snow and Landscape Research (WSL), Birmensdorf, CH-8903, Switzerland

<sup>5</sup>Department of Geosciences, University of Fribourg, Fribourg, 1700, Switzerland

<sup>6</sup>Department of Earth Science and the Bjerknes Centre for Climate Research, University of Bergen, 5020, Norway

<sup>7</sup>Statkraft, Gaupne, 6868, Norway

<sup>8</sup>Breheimsenteret, Jostedal, 6871, Norway

<sup>9</sup>COWI, Bergen, 5824, Norway

<sup>10</sup>Norgesguidene, Jostedal, 6871, Norway

*Correspondence to:* Mette Kusk Gillespie (mette.kusk.gillespie@hvl.no)

**Abstract.** We present an extensive dataset of ice thickness measurements from Jostedalsbreen ice cap, mainland Europe's largest glacier. The dataset consists of more than 351 000 point values of ice thickness distributed along ~1100 km profile segments that cover most of the ice cap. Ice thickness was measured during field campaigns in 2018, 2021, 2022, and 2023 using various ground-penetrating radar (GPR) systems with frequencies ranging between 2.5 and 500 MHz. The large majority of ice thickness observations were collected in spring using either snowmobiles (90 %) or a helicopter-based radar system (8 %), while summer measurements were carried out on foot (2 %). To ensure accessibility and ease of use, metadata were attributed following the GlaThiDa dataset ([GlaThiDa Consortium, 2020](#)) and follows the FAIR (Findable, Accessible, Interoperable, and Reusable) guiding principles. Our findings show that glacier ice of more than 400 m thickness is found in the upper regions of large outlet glaciers, with a maximum ice thickness of ~630 m in the [accumulation area of Tunsbergdalsbreen-outlet glacier-accumulation-area](#). Thin ice of less than 50 m covers narrow regions joining the central part of Jostedalsbreen with its northern and southern parts, making the ice cap vulnerable to break-up with future climate warming. Using the point values of ice thickness as input to an [iceice](#) thickness model, we compute 10 m grids of ice thickness and bed topography that cover the entire ice cap. From these distributed datasets we find that Jostedalsbreen has a mean ice thickness of 154 m  $\pm$ 22 m and a present (~2020) ice volume of 70.6  $\pm$ 10.2 km<sup>3</sup>. Locations of depressions in the map of bed topography are used to delimitate the locations of potential future lakes,

36 consequently providing a glimpse of the landscape if the entire Jostedalsgreen melts away. Together, the  
37 comprehensive ice thickness point values and ice cap-wide grids serve as a baseline for future climate change  
38 impact studies at Jostedalsgreen.  
39 All data are available for download at <https://doi.org/10.58059/yhwr-rx55> (Gillespie et al., 2024).

## 40 **1 Introduction**

41 Global glacier mass loss caused by increased atmospheric temperatures and associated processes contributes  
42 significantly to changes in sea level, water resources and natural hazards (IPCC, 2021). Projections of future  
43 changes show that glaciers and ice caps will continue to lose mass due to anthropogenic warming, and that the  
44 majority of the world's glaciers and ice caps are at risk of being lost by 2100 (Rounce et al., 2023). However, global  
45 glacier projections remain uncertain. This is especially true for ice caps, where model efforts of ice thickness  
46 distribution in the flat upper regions and across ice divides represents a particular challenge (Millan et al., 2022;  
47 Frank et al., 2023).

48  
49 Information on ice thickness distribution of a glacier is a prerequisite for accurate modelling of ice dynamics and  
50 glacier evolution, as well as future hydrological impacts. Ice thickness measurements are also essential for precise  
51 calculations of the ice volume of glaciers and in mapping of the subglacial topography. Consequently, significant  
52 efforts have been made to compile ice thickness data and provide grids of ice thickness and bed topography (e.g.,  
53 Gärtner-Roer et al., 2014; Lindbäck et al., 2018; Frémand et al., 2023). The third version of the Glacier Thickness  
54 Database (GlaThiDa v3) includes nearly 4 million ice thickness measurements distributed over roughly 3000  
55 glaciers worldwide, and 14 % of the world's glacierized area is now within 1 km of an ice thickness measurement  
56 (GlaThiDa Consortium, 2020; Welty et al., 2020). Direct inter- and extrapolation of ice thickness measurements  
57 with various techniques, such as kriging, inverse-distance weighting, or spline interpolations (Flowers and Clarke,  
58 1999; Binder et al., 2009; Fischer, 2009; Yde et al., 2014; Andreassen et al., 2015) is possible, but may produce  
59 large uncertainties in areas without measurements (Gillespie et al., 2023). Consequently, ice thickness modelling  
60 is necessary to extrapolate measurements more accurately to unmeasured regions (Andreassen et al., 2015;  
61 Farinotti et al., 2021), and to infer ice thickness for glaciers without direct measurements.

62  
63 Various ice thickness inversion approaches exist that do not require bed topography or ice thickness as input (e.g.,  
64 Huss and Farinotti et al., 2012; Linsbauer et al., 2012; ~~Fürst et al., 2017~~; Farinotti et al., 2019; Frank et al., 2023),  
65 and recent efforts to model ice thickness through inversion of surface topography have made distributed ice  
66 thickness information available for every individual glacier in the world (Farinotti et al., 2019; Millan et al., 2022) and  
67 all Scandinavian glaciers and ice caps (Frank and van Pelt, 2024). Although ice thickness observations are not

68 required as input in these models, databases of ice thickness, when available, remain important for calibration and  
69 validation of model behaviour. Assessments of model performances, such as the first Ice Thickness Model  
70 Intercomparison eXperiment (ITMIX; Farinotti et al., 2017), found that model output is highly variable, and that the  
71 best results are achieved when using model ensembles. In addition, a more recent model comparison (ITMIX2;  
72 Farinotti et al., 2021) demonstrated the added value of in situ ice thickness observations to constrain models. A  
73 limited set of ice thickness observations, preferably from the thickest parts of the glacier, ~~provided were~~ efficient ~~in~~  
74 ~~constraining to constrain~~ mean glacier thickness, illustrating that even sparse ice thickness observations are of  
75 importance in ice thickness modelling. Consequently, readily accessible ice thickness observations for calibration  
76 and validation ~~remains remain~~ key for developing a new generation of ice thickness estimation models (Farinotti et  
77 al., 2017). ~~Measurements across the flat upper regions of ice caps such as Jostedalsgreen are of particular value,~~  
78 ~~as these can be applied to improve ice thickness models for the much larger ice sheets in Greenland and Antarctica,~~  
79 ~~and ultimately facilitate more accurate predictions of future sea-level change (Morlighem et al., 2017)-2017).~~

80

81 In Norway, numerous field campaigns to measure ice thickness have been carried out over the years (Andreassen  
82 et al., 2015). The purpose of the earliest measurements was typically to determine subglacial topography in relation  
83 to hydropower planning, such as subglacial intakes and water divides (e.g., Kennett, 1989; 1990), or detailed  
84 studies related to jökulhlaups (Engeset et al., 2005). While the first attempts at ice thickness mapping used seismic  
85 measurements (e.g., Sellevold and Kloster, 1964) or hot water drilling (e.g., Østrem et al., 1976), from 1980 ground-  
86 penetrating radar (GPR) has been the preferred method for largescale mapping of glaciers in Norway (e.g.,  
87 Sætrang and Wold, 1986). Since these first radar measurements on Norwegian glaciers, technological  
88 advancements in radar systems, processing techniques and positioning accuracy have enabled the use of GPR in  
89 a wide range of glaciological applications, such as mapping of ice- or snow thickness, internal layering, thermal  
90 regime, or englacial meltwater channels (e.g., Plewes and Hubbard, 2001; Dowdeswell and Evans, 2004; Navarro  
91 and Eisen, 2009). The penetration depth and level of detail in GPR data are determined by the antenna frequency.  
92 Information on ice and snow characteristics can be achieved by using very-high (30–300 MHz) or ultra-high (300–  
93 3000 MHz) antenna frequencies, while high-frequency GPR surveys (3–30 MHz antenna frequency) have larger  
94 penetration depth at the expense of resolution (Schlegel et al., 2022). High-frequency antennas are consequently  
95 the better choice in surveys of bed topography and grids of glacier geometry based on such measurements have  
96 been widely used to model future changes in Norwegian glaciers (e.g., Laumann and Nesje, 2009, 2014; Giesen  
97 et al., 2010; Åkesson et al., 2017, Johansson et al., 2022).

98

99 Jostedalsgreen is the largest ice cap in mainland Europe and makes up about 20 % of the total glacierized area of  
100 mainland Norway (Andreassen et al., 2022). The effect of global warming is evident in the region and monitored  
101 outlet glaciers flowing from the ice cap have thinned and retreated with increased speed since 2000 (e.g.,

102 Andreassen et al., 2020; Seier et al., 2024). The effects of future warming on accessibility, glacier-atmosphere  
103 systems and hydrology are likely to significantly impact regional businesses such as agriculture, tourism, and  
104 hydropower production. Despite the importance of Jostedalsgreen to both regional stakeholders and the scientific  
105 community, the natural and societal consequences of climate-forced changes in the region remain largely unknown.  
106 Future changes of Jostedalsgreen can be assessed through glacier evolution modelling, but accurate results  
107 require high-quality information on ice thickness and bed topography as model input (Farinotti et al., 2017).  
108 Although several surveys of ice thickness were conducted on Jostedalsgreen during the 1970s and 1980s (e.g.,  
109 Østrem et al., 1976; Andreassen et al., 2015), prior to the new ice thickness measurements described in this paper,  
110 many parts of the ice cap had either poor or no data coverage.

111  
112 Here we present a comprehensive and up-to-date point dataset of ice thicknesses of Jostedalsgreen measured by  
113 GPR during the period 2018–2023. Ice thickness measurements were predominantly performed on the glacier  
114 surface (ground-based), but in regions that were inaccessible on the ground we applied a helicopter (airborne)  
115 radar system. We used antenna frequencies ranging from 2.5 to 500 MHz to capture the thickness of the ice in the  
116 best possible resolution. For regions that remain unmeasured due to resource or accessibility constraints, we use  
117 ~~interpolation and~~ inter- and extrapolation of the direct measurements in connection with locally constrained ice  
118 thickness modelling to provide new grids of ice thickness and bed topography for the entire ice cap. Depressions  
119 in the subglacial bed topography grid are used to infer the locations of lakes if Jostedalsgreen disappeared  
120 completely from the landscape. We provide a thorough description of the uncertainties associated with ice thickness  
121 measurements and modelling results, including comprehensive uncertainty estimates. The enhanced datasets on  
122 Jostedalsgreen ice thickness and bed topography have the potential to significantly advance modelling efforts for  
123 the past and future evolution of the ice cap and provide accurate assessments of regional climate change impact.  
124 In addition, comprehensive high-accuracy measurements over the complex glacier geometry at Jostedalsgreen  
125 constitute a valuable resource for improving current ice thickness models, particularly on ice caps, where the flat  
126 upper regions and discontinuities across ice divides provide a special challenge.

## 127 **2 Study site**

128 Jostedalsgreen (Fig. 1) has an area of 458 km<sup>2</sup> and an elevation ranging between 380 and 2006 m a.s.l.  
129 (Andreassen et al., 2022). The climate is subarctic to tundra with a mean annual air temperature of -3°C at 1633  
130 m a.s.l. (2009–2022 average at Steinmann meteorological station; (Fig. 1); Engen et al., in-review2024). In the  
131 most recent national glacier inventory, Jostedalsgreen is divided into 81 glacier units from observations of  
132 topographic ice divides (Andreassen et al., 2022). Many of these glacier units have individual names which will be  
133 referred to throughout this paper. Jostedalsgreen is defined as a single ice cap but can geographically be divided

134 into three minor ice caps that are currently connected (Fig. 1). In this paper, we refer to Jostedalsbreen South  
135 (south of Grensevarden), Central (north of Grensevarden as far as and including [the glacier Lodalsbreen-glacier](#))  
136 and North (northeast of [Lodalsbreen-glacier](#)).  
137

138 Jostedalsbreen reached its maximum Little Ice Age (LIA) extent between 1740 and 1860 CE with an estimated  
139 area of 572 km<sup>2</sup> (Carrivick et al., 2022; Andreassen et al., 2023). Since then, the ice cap has experienced an overall  
140 reduction in size, interrupted temporarily by advances in several fast-responding outlet glaciers, the latest of which  
141 occurred in the 1990s due to increased winter precipitation (Nesje et al., 1995; Andreassen et al., 2005). By 2006,  
142 the major outlet glaciers had in combination lost at least 93 km<sup>2</sup> or 16 % of their LIA area and 14 km<sup>3</sup> or 18 % of  
143 their LIA volume (Carrivick et al., 2022). Increasing summer temperatures further reduced the glacier area by 3 %  
144 from 2006 to 2019 (Andreassen et al., 2022) and continues to [do so to](#) this day (Seier et al. 2024). Overall, the  
145 change in the glacial landscape has been considerable, with measurements of glacier front variation (length  
146 changes) at several outlet glaciers revealing a total reduction in length of 1–3 km since ~1900 (Andreassen et al.,  
147 2023), of which 300–700 m has occurred since 2000 (Kjøllmoen et al., in prep.).  
148

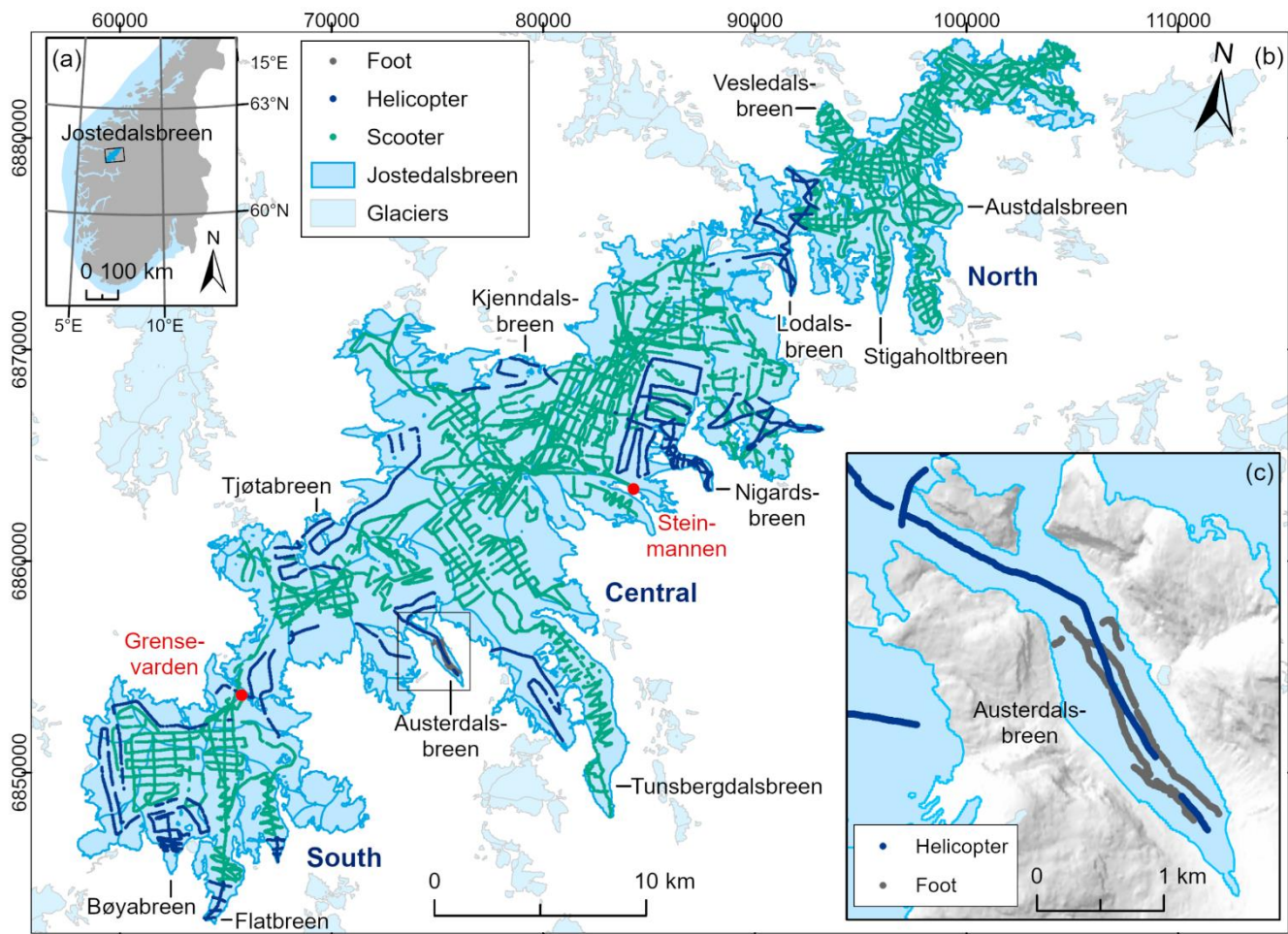
149 The first ice thickness measurements on Jostedalsbreen were conducted in 1973 along two cross profiles located  
150 between 700 and 800 m a.s.l. on the tongue of [Nigardsbreen](#) the outlet glacier [Nigardsbreen](#) (Østrem et al., 1976).  
151 In total, 14 points were drilled using electrical hot-point drilling, revealing ice thicknesses of up to 200 m. In 1986  
152 hot water drilling was carried out on [Bødalsbreen](#) the outlet glacier [Bødalsbreen](#) along three cross profiles at 780–  
153 815 m a.s.l. (Haakensen and Wold, 1986). Results from 15 boreholes show that ice thickness varied between 50  
154 and 60 m in this region. GPR was first used on Jostedalsbreen in the 1980s during field campaigns on Nigardsbreen  
155 and surrounding glaciers in 1981, 1984, and 1985 (Sætrang and Wold, 1986), on Austdalsbreen and surrounding  
156 glaciers in 1986 (Sætrang and Holmqvist, 1987), and south of Nigardsbreen in 1989 (Andreassen et al., 2015).  
157 Results show that ice thickness along transects typically varied between 150 and 300 m, with ice of up to 600 m in  
158 the flattest regions and thinner ice (50–100 m) at the highest points of the ice cap (Sætrang and Wold, 1986).  
159 These early measurements of ice thickness are associated with relatively large uncertainties in surface elevations  
160 and the positioning of GPR profiles. In addition, as data were collected and processed with analogue techniques,  
161 only parts of the older dataset are available digitally. Digitised data from these campaigns have been submitted to  
162 the GlaThiDa database (GlaThiDa Consortium, 2020; Welty et al., 2020) and were used by Andreassen et al.  
163 (2015) to interpolate ice thickness distribution and estimate a mean ice thickness of 158 m for parts of  
164 Jostedalsbreen (65 % of total area). More recently, Jostedalsbreen was included in a modelling study of ice volume  
165 and thickness distribution of all Scandinavian glaciers (Frank and van Pelt, 2024). In this study, existing ice  
166 thickness measurements were used to calibrate an ice [thickness](#) [thickness](#) model, resulting in a total volume of  
167 72.6 km<sup>3</sup> for Jostedalsbreen.

## 168 **3 Methods and data**

### 169 **3.1 Ice thickness measurements**

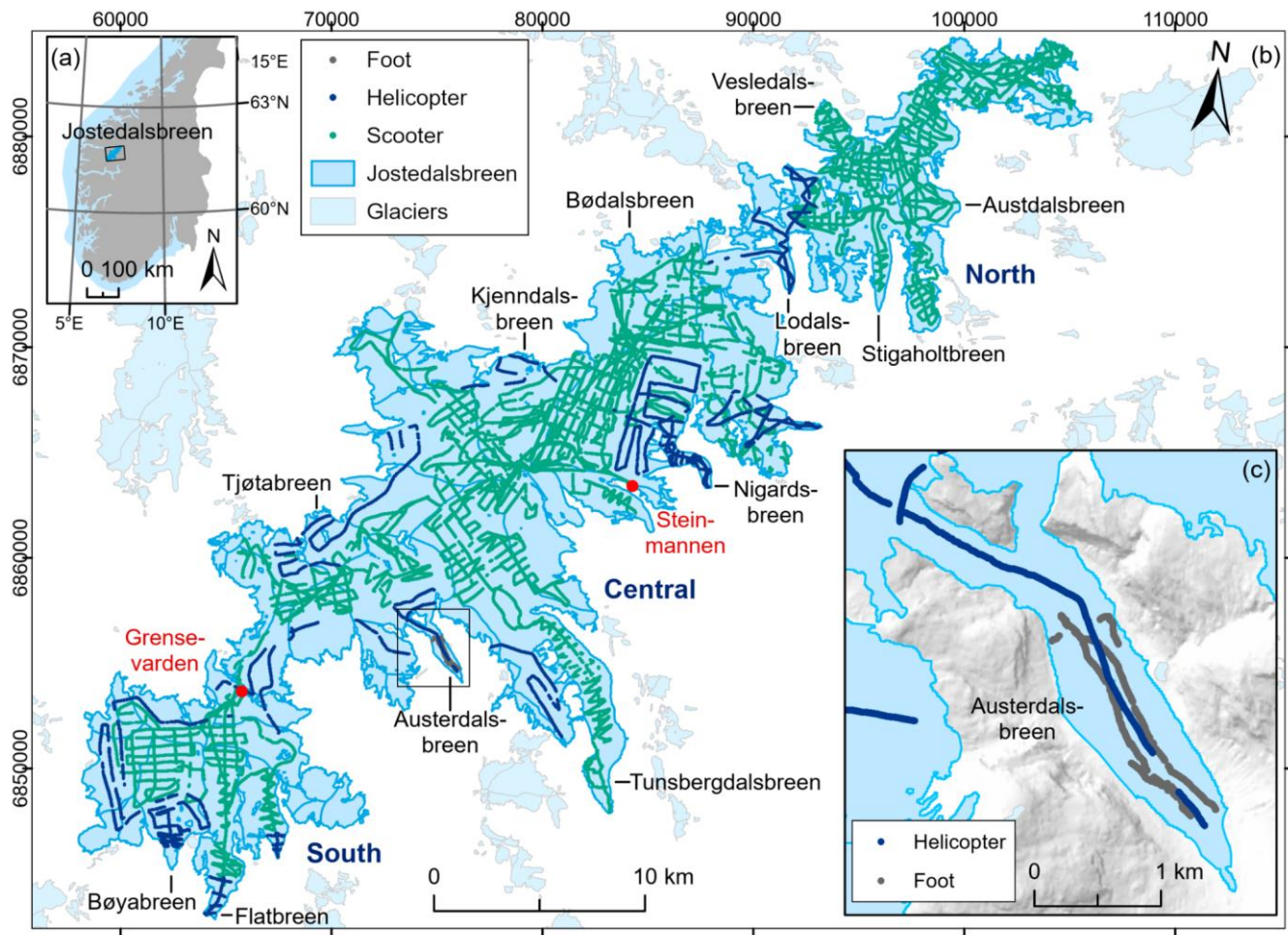
170 The ice thickness measurements presented in this paper were collected during field campaigns between 2018 and  
171 2023. The first measurements were carried out in April 2018, however most of the data were gathered in April  
172 2021, March to April 2022 and April 2023 (Fig. [A4A1a](#)), while the tongue of Austerdalsbreen was surveyed in  
173 September 2021. The principle means of transport during data collection was snowmobile (90 % of all datapoints),  
174 but a ~~newly developed~~new helicopter radar system (Air-IPR) [based on the ground-based Blue System Integration](#)  
175 [Ltd. IceRadar \(Mingo and Flowers, 2010\)](#) was deployed ~~in~~for steep and crevassed regions of the ice cap (8 % of  
176 all datapoints). Summer measurements on foot account for only 2 % of all datapoints (Fig. 2). Although airborne  
177 surveys were quicker, ground-based measurements were preferred whenever possible due to the generally better  
178 data quality caused by lower travel speeds, less noise (electronic and off nadir-reflections) and simpler wave  
179 propagation (lack of an air layer). Depending on the surface conditions, we collected the data in a grid pattern, with  
180 the main profiles spaced no more than 400 m apart and oriented transverse to the ice flow direction. Survey lines  
181 perpendicular to main profiles were 400–800 m apart, depending on accessibility and time constrains during the  
182 fieldwork. In total, we have successfully detected the glacier bed along ~920 km of profile segments collected with  
183 the ground-based radar systems and ~170 km of profile segments collected with the airborne radar system (Fig.  
184 1). Following the new measurements, 90 % of the ice cap is now less than 300 m from an observation of ice  
185 thickness (measurement or glacier outline) and 49 % is within 100 m of a known point.

186



187

188



189

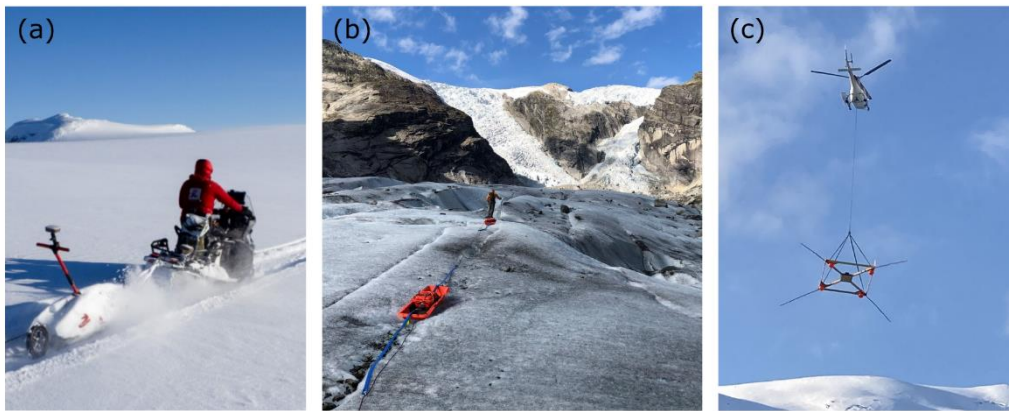
190 **Figure 4-1:** Map showing (a) the location of Jostedalsbreen in southern Norway, (b) Jostedalsbreen and GPR surveys  
 191 divided into helicopter, snowmobile, and foot, with red dots indicating locations referenced in the text, and (c) the  
 192 measurements on Austerdalsbreen by foot and helicopter. The shown glacier extent and outline outlines of glacier  
 193 units are from 2019 (Andreassen et al., 2022). Background mountain shadow on (c) is from the 100 m national DTM by  
 194 the Norwegian Mapping Authority. The coordinate systems are geographical coordinates on (a) and UTM 33N, datum  
 195 ETRS89 on (b) and (c).

196

197 Based on the terminology proposed by Schlegel et al. (2023), we used a combination of high, very high and ultra-  
 198 high frequency radar systems to gather detailed information on snow, firn and shallow ice, while maintaining a good  
 199 penetration depth for deep ice. Usually two snowmobiles would travel together, one towing a high frequency  
 200 generation 1–3 Blue System Integration Ltd. IceRadar system with 2.5 or 5 MHz antennas (Mingo and Flowers,  
 201 2010) depending on the ice thickness in the investigated area, and the other snowmobile towing either a higher  
 202 frequency Malå GPR system with 25 or 50 MHz rough terrain antennas, or 450 or 500 MHz shielded antennas  
 203 (Table 1). On one occasion, measurements were conducted using a Radarteam GPR system with a 40 MHz



204 monostatic antenna and an upgraded non-commercial GPR with 5 MHz antennas (NVE-radar), similar to that  
205 described by Sverrisson et al. (1980) and Pettersson et al. (2011). For the measurements on foot on the tongue of  
206 Austerdalsbreen, we chose a 10 MHz Blue System Integration Ltd. IceRadar and a 50 MHz Malå GPR. All  
207 helicopter measurements were collected using a 5 MHz Air-IPR Generation 3 Blue System Integration Ltd.  
208 IceRadar system with the antennas in a V dipole configuration (Table 1). The carrying platform for the Air-IPR is  
209 built with wood and uses telescopic rods in composite material to hold the antennas (Fig. 2c). To ~~secure an~~  
210 ~~accurate~~ ensure a  $\sim 30$  m distance between the antennas and the ice surface, we used a laser mounted on the  
211 platform with a wireless connection to the cockpit. ~~The~~ Travel speed during the helicopter measurements was  $\sim 10$   
212 ~~m s<sup>-1</sup> and the~~ control of the IceRadar during both ground-based and airborne measurements was performed using  
213 a tablet and a remote connection.



215  
216 **Figure 2: Data collection was undertaken (a) by snowmobile, (b) on foot, and (c) by helicopter. Photos: (a) Kjetil Melvold,**  
217 **(b) Mette K. Gillespie and (c) Torgeir O. Røthe.**

218  
219 Ground-based measurements of ice thickness were largely carried out using an in-line antenna configuration with  
220 distances between receiver (Rx) and transmitter (Tx) units depending on the antenna frequency and varying from  
221 4 m (50 MHz) and 6.5 m (25 MHz) for the two Malå rough terrain antennas to 15 m (10 MHz), 30 m (5 MHz) and  
222 60 m (2.5 MHz) for the three IceRadar antenna sets. The 5 MHz NVE-radar antennas were also run using an in-  
223 line configuration, but with 32 m between antenna mid-points. By contrast, the shielded 450 MHz and 500 MHz  
224 Malå antennas were oriented perpendicular to the travel direction and with a 0.18 m antenna separation. To avoid  
225 interference between radar systems during data collection, the two snowmobiles travelled at a distance of more  
226 than 50 m. For frequencies of 25 MHz and above, each measurement (trace) was stacked between 4 and 8 times  
227 to increase the signal-to-noise ratio, whereas the 2.5 and 5 MHz measurements were stacked 256 times. Ice  
228 thickness measurements were collected at a constant time interval, which varied according to limitations in the

229 different radar systems. The distance between individual traces along radar profiles was affected by this and our  
 230 travel speed ( $\sim 15 \text{ km h}^{-1}$ ). Measurements collected with antenna frequencies ranging between 25 and 500 MHz  
 231 were sampled at the highest rate (trace distances of  $\sim 0.2\text{--}2 \text{ m}$ ). Therefore, while these measurements constitute  
 232 a significant proportion of total datapoints (Table 1), the vast majority of data coverage is attributed to ice thickness  
 233 observations along 5 and 2.5 MHz profiles, which were collected less densely. In general, ground-based  
 234 measurements of ice thickness were registered at intervals ranging between 3 and 6 m, while airborne  
 235 measurements were 3 to 20 m apart. GNSS locations along survey lines were recorded every 1 s with a horizontal  
 236 positioning accuracy of up to 5 m for the Malå radar system (G-Star IV BU-353S4 receiver) and 3 m for the IceRadar  
 237 system (Garmin GPSx OEM sensor). In addition, differential GNSS (DGNSS) measurements were carried out  
 238 independently of the radar measurements in some regions.

239

240 **Table 1: Survey dates and equipment used for ice thickness measurements during the 2018–2023 field campaigns. The**  
 241 **number of datapoints refers to the post-processed and interpreted dataset. Institutions are Western Norway University**  
 242 **of Applied Sciences (HVL), the Norwegian Water Resources and Energy Directorate (NVE) and University of Bergen**  
 243 **(UIB).**

Method	Radar type	Frequency	Points	Survey dates	Institutions	
<i>Ground-based radar</i>	IceRadar	2.5 MHz	15712	18–19 April 2018	HVL	
	NVE-radar	5 MHz	18569	18 April 2018	NVE	
	IceRadar Malå GPR Malå GPR	2.5 and 5 MHz 50 MHz RTA 450 MHz shielded	99745 4503 15308	11–18 April 2021	HVL	
	RadarTeam Subecho 40	40 MHz	32533	16–17 April 2021	NVE	
	IceRadar Malå GPR	2.5 MHz 25 MHz RTA	5221 5753	20–24 April 2021	UIB	
	IceRadar Malå GPR	10 MHz 50 MHz RTA	4825 2723	4 September 2021	HVL	
	IceRadar	5 MHz	11769	8 March 2022	HVL	
	IceRadar Malå GPR	5 MHz 25 and 50 MHz RTA	18424 11938	19–22 March 2022	HVL	
	IceRadar	5 MHz	5856	5–6 April 2022	NVE	
	IceRadar Malå GPR Malå GPR	5 MHz 50 MHz RTA 500 MHz shielded	53061 12509 4282	20–21 April 2022	HVL	
	IceRadar	2.5 MHz	621	22 March 2023	HVL	
	<i>Airborne radar</i>	IceRadar	5 MHz	5725	22 March 2022	UIB
		IceRadar	5 MHz	5151	7 April 2022	UIB and HVL
		IceRadar	5 MHz	5267	26 April 2022	HVL
		IceRadar	5 MHz	12064	20 April 2023	HVL

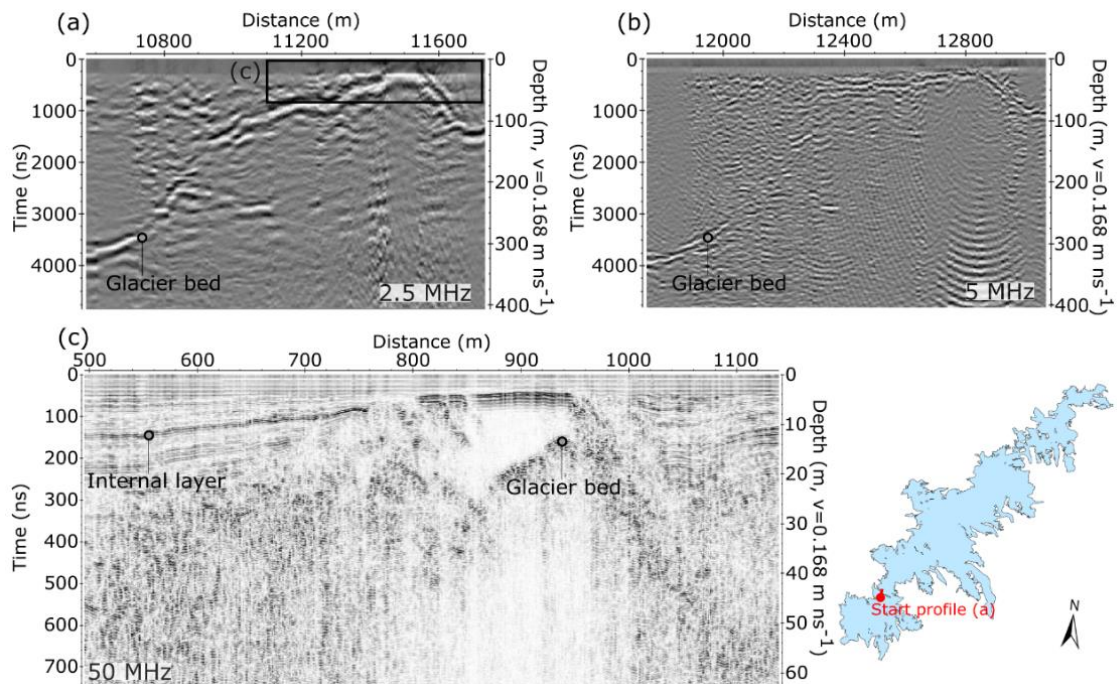
244

### 245 3.2 Data processing and interpretation

246 The raw GPR data was primarily processed using the ReflexW module for 2D data analysis (Sandmeier Scientific  
247 Software, version 8.5). Initial data processing involved adding GNSS positions for antenna midpoints to all traces,  
248 merging individual shorter profiles into larger segments, and assigning a constant trace increment along each  
249 segment to allow for subsequent migration. We chose a trace increment close to the mean value during travel to  
250 avoid deleting or introducing too many traces to the original dataset. Following the initial data sorting, we used a  
251 combination of 1) dewow, 2) Butterworth bandpass filtering, 3) time zero correction, 4) dynamic correction, 5)  
252 energy decay gain, and 6) f-k Stolt migration on all ground-based measurements. For the GPR measurements  
253 collected with 2.5 and 5 MHz systems, processing steps 3) and 4) are important to account for the influence of the  
254 large antenna separation on first signal arrival times and the radar wave path through the ice. Further filtering was  
255 required on the airborne measurements due to significant system-related noise. The processing routine for this  
256 portion of the dataset consequently involved applying an adaptive filter using the IceRadarAnalyzer processing  
257 software (Blue System Integration Ltd., version 6.3.1. beta) to remove unwanted signals from the radar profiles, in  
258 addition to dewow and bandpass filtering. Subsequent static correction was undertaken in ReflexW using manually  
259 delineated arrival times of the glacier surface reflection, after which energy decay gain and f-k Stolt migration were  
260 applied.

261  
262 Following data processing, we observed a bed reflection along most 2.5 and 5 MHz radar segments and in higher  
263 frequency measurements collected in ice-marginal regions (Fig. 3). The bed reflections were delineated manually,  
264 and we calculated ice thickness from the reflection two-way travel time by assuming a constant radio-wave velocity  
265 in ice of  $0.168 \text{ m ns}^{-1}$ , similar to that used on other glaciers in Norway and abroad (Dowdeswell and Evans, 2004;  
266 Navarro and Eisen, 2009; Andreassen et al., 2012a; Yde et al., 2014; Johansson et al., 2022).

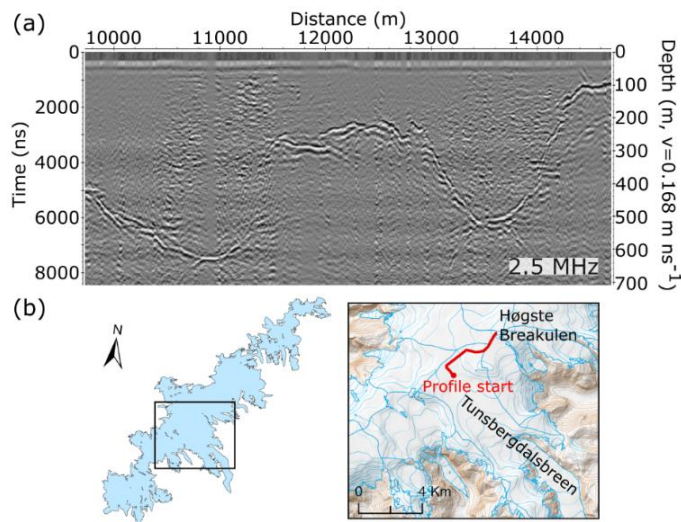
267



268  
 269 **Figure 3: Example of measurements with (a) 2.5 MHz, (b) 5 MHz and (c) 50 MHz antennas on shallow ice along a profile**  
 270 **travelling north near Grensevarden (Fig. 1). The 2.5 and 50 MHz profiles were collected along identical tracks in 2021,**  
 271 **while the 5 MHz measurements are from 2022 along a profile located ~50 m from these tracks. The radargrams illustrate**  
 272 **well the difference in resolution and penetration depth resulting from variations in antenna frequency. The lowest**  
 273 **frequency measurements provide information on bed topography along the entire profile, while the 50 MHz profile**  
 274 **allows for accurate measurements of thin ice and offers evidence of internal ice characteristics.**

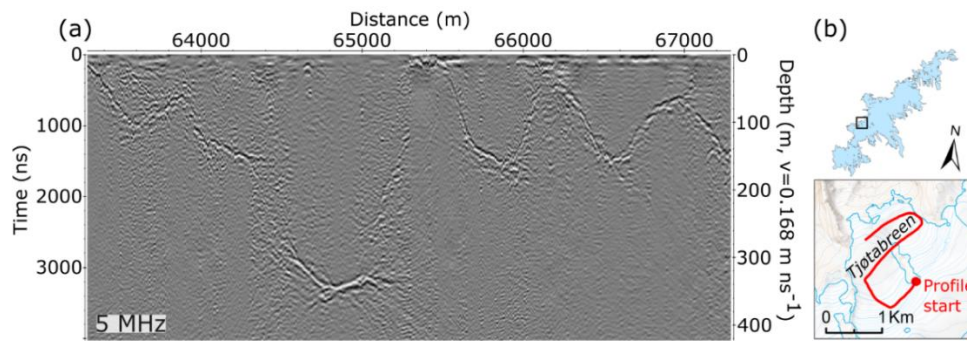
275  
 276 ~~Following data processing, we observed a bed reflection along most 2.5 and 5 MHz radar segments and in higher~~  
 277 ~~frequency measurements collected in ice marginal regions (Fig. 3). The bed reflections were delineated manually,~~  
 278 ~~and we calculated ice thickness from the reflection two-way travel time by assuming a constant radio wave velocity~~  
 279 ~~in ice of  $0.168 \text{ m ns}^{-1}$ , similar to that used on other glaciers in Norway and abroad (Dowdeswell and Evans, 2004;~~  
 280 ~~Navarro and Eison, 2000; Andreassen et al., 2012a; Yde et al., 2014; Johansson et al., 2022).~~ The range of  
 281 frequencies allows for a detailed mapping of both shallow and deep ice at the best possible resolution. In shallow  
 282 regions, ice thickness was most accurately determined from the highest frequency measurements, which also  
 283 provide information on snow (450 and 500 MHz data only), firn and internal layer characteristics (Fig. 3c). In this  
 284 paper, we present only the interpreted ice thickness from these higher frequency measurements. In general, GPR  
 285 measurements at Jostedalbreen are characterised by strong scattering and rapid attenuation of the radar signal  
 286 (Fig. 3c), as is typical for radar surveys on temperate glaciers (Smith and Evans, 1972; Ogier et al., 2023).  
 287 Occasionally, regions of more transparent ice were observed in the higher frequency measurements (Fig. 3c).  
 288 These likely indicate either zones that are above the internal water table or isolated patches of cold (frozen) ice.

289 While the 5 MHz antennas generally performed well in depths of up to 400–500 m, the advantage of using 2.5 MHz  
290 antennas was evident in areas with sloping bed topography (Fig. 3a and 3b) and in the deepest regions, where  
291 reflectors were sometimes weak or absent, even with the 2.5 MHz system (Fig. 4).  
292



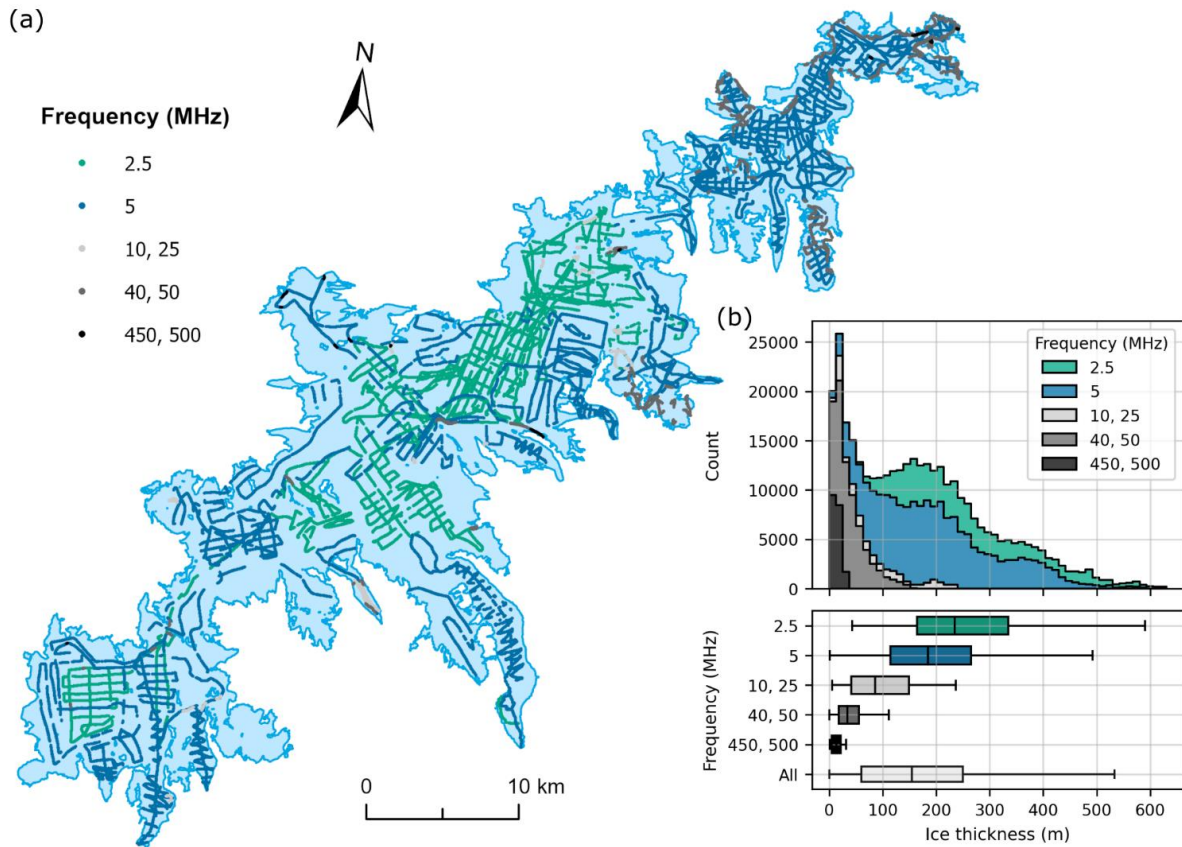
293  
294 **Figure 4: (a) Example radargram of measurements with 2.5 MHz antennas. (b) The profile was located along a transect**  
295 **in the upper part of Tunsbergdalsbreen (Fig. 1), where the thickest ice was observed. The detailed background map in**  
296 **(b) is from the Norwegian Mapping Authority (WMS for Topografisk Norgeskart available at <https://www.geonorge.no/>)**  
297 **and the 2019 [outlineoutlines](#) of glacier units on (b) [isare](#) from Andreassen et al. (2022).**

298  
299 The efficiency of snowmobile transport during the fieldwork depended strongly on the snow conditions and varied  
300 significantly between field seasons. For example, valley access onto Tunsbergdalsbreen was possible in 2022,  
301 when the snow cover was thick, but attempts to drive onto the glacier tongue in 2023 had to be abandoned. The  
302 helicopter measurements generally cover regions that were inaccessible on snowmobile, either due to steep and/or  
303 crevassed terrain, or unfavourable snow conditions. Consequently, helicopter measurements provide a valuable  
304 addition to the ground-based measurements. However, the airborne measurements generally had a lower  
305 penetration depth than ground-based measurements using the same antenna frequency, primarily due to increased  
306 electronic noise and radar wave attenuation, as well as scattering of the radar signal caused by large surface  
307 crevasses present in many airborne surveyed regions. Despite these challenges, bed reflectors were generally  
308 observed at depths of up to 350–400 m of ice in airborne measurements (Fig. 5B1).  
309  
310



311 **Figure 5:** (a) Example of measurements with the 5 MHz airborne radar system. (b) The profile was located along a  
 312 transect at Tjøtabreen (Fig. 1). The background map in (b) is from the Norwegian Mapping Authority (WMS for  
 313 Topografisk Norgeskart available at <https://www.geonorge.no/>) and the 2019 glacier outline is from Andreassen et al.  
 314 (2022).  
 315

316  
 317 After the initial ice thickness calculations, all observations of ice thickness were plotted in ArcGIS Pro, where we  
 318 deleted points collected with the 5 and 2.5 MHz radar systems in sharp turns, as the long antennas were not fully  
 319 extended in these locations. Profile lines collected alongside and in close proximity to valley walls were also  
 320 removed to limit the influence of off-nadir reflections in the dataset. In marginal regions with both high- and ultra-  
 321 high frequency observations, high-frequency measurements (2.5 and 5 MHz) were deleted due to their comparably  
 322 lower accuracy. In order to produce a consistent dataset of ice thicknesses for the entire Jostedalsbreen, we  
 323 double-checked interpretations at all locations where ice thickness observations from crossing profiles differed by  
 324 more than 15 m. When contrasting observations suggested that a transect was influenced by off-nadir reflectors or  
 325 other uncertainties such as resolution issues, the presence of multiple reflectors or location uncertainties, these  
 326 datapoints were removed from the dataset. The combination of multiple frequency measurements in many regions  
 327 of the ice cap has resulted in a dataset where both thin and very thick ice is represented in a generally satisfactory  
 328 resolution (Fig. 65).  
 329



330

331 **Figure 65:** (a) Ice thickness measurements across Jostedalsglaciären categorized according to antenna frequency. The  
 332 thickest regions of the ice cap were measured using the lowest frequency antennas, while higher frequencies were  
 333 applied in the more marginal and thinner regions. (b) Histogram (top) and boxplot (bottom) of measurements of ice  
 334 thickness categorised by antenna frequency. Boxes represent the interquartile range (IQR; the spread of the middle  
 335 50 % of the data), with medians indicated by vertical lines. Whiskers extend to the highest and lowest values that are  
 336 within the 1.5\*IQR limits. The analysis shows that measurements collected using higher frequency GPR systems  
 337 dominate at low ice thickness, while 5 and 2.5 MHz GPR systems were the better choice for ice thicknesses above ~100  
 338 m.

### 339 3.3 Homogenization to 2020 DTM and calculation of glacier bed topography

340 Following the data processing and interpretation of the GPR measurements, the bed topography elevation beneath  
 341 Jostedalsglaciären was calculated from the point values of ice thickness and a recent 10 m national digital terrain  
 342 model (DTM10) from the Norwegian Mapping Authority. For Jostedalsglaciären, the DTM10 is derived from airborne  
 343 laser scanning (lidar) collected by Terratec over a seven-day period in August 2020, that covered Jostedalsglaciären  
 344 and surrounding area with a point density of minimum 2 pp m<sup>-2</sup> (Terratec, 2020). The central part of the ice cap  
 345 was scanned on 9 August, the western part on 10 August and the eastern part on 15 August. The accuracy of the  
 346 final point cloud is assumed to be ±0.1 m (Andreassen et al., 2023). The 2020 survey (2020 DTM) covers the entire

347 Jostedalsbreen, except for the lower tongue of Tunsbergdalsbreen (Andreassen et al., 2023) where surface  
348 elevation data in DTM10 is derived from stereophotogrammetry using 2017 orthophotos.

349

350 To prevent discontinuities in the elevation of bed topography, all ice thickness measurements were homogenised  
351 to correspond to the date of the 2020 DTM. We used DGNSS observations of surface elevation to calculate an  
352 area dependent mean surface elevation difference between the time of acquisition of GPR data and the 2020 DTM.  
353 Calculations show that DGNSS measurements exceed the DTM by average values ranging from 0.6 m (northern  
354 parts in spring 2022) to 3.9 m (central parts in spring 2018), reflecting surface changes such as the increased depth  
355 of the snowpack during spring measurements compared to the end of summer lidar scan. The elevation of the bed  
356 topography was calculated by subtracting the homogenised ice thicknesses from the 2020 DTM.

### 357 **3.4 Ice thickness measurement uncertainties**

358 The multifrequency dataset of crossing profiles allows for an investigation of discrepancies between measurements  
359 with various degrees of vertical resolution as a means to evaluate ice thickness uncertainties. Here, we present the  
360 results of a comparison of ice thicknesses at intersection points (crossover analysis), in addition to the total  
361 calculated measurement uncertainty for each datapoint following the method described by Lapazaran et al. (2016).  
362 In the final dataset, profiles crossed at 1207 locations (not counting profiles collected along identical tracks). Ice  
363 thicknesses in crossing points had a mean absolute difference (MD) of 6.8 m with a standard deviation (SD) of 5.8  
364 m, which when expressed in relation to ice thickness equals a MD of 5.0 % (7.1 % SD). Not surprisingly, the  
365 discrepancy between values increased with decreasing frequency and hence vertical and horizontal resolution.  
366 The largest discrepancies were observed where at least one of the crossing profiles was collected with 2.5 MHz  
367 antennas (MD of 8.4 m and a 6.7 m SD; maximum discrepancy of 39 m; n=538), whereas profiles collected with  
368 500 and 450 MHz antennas generally corresponded better with other observations (MD of 3.7 m and a 3.1 m SD;  
369 maximum discrepancy of 10 m; n=23). The crossover analysis also facilitated an assessment of the performance  
370 of the lowest frequency measurements when compared to higher resolution and more accurate ice thickness  
371 observations collected using antenna frequencies of 25–500 MHz. The comparison show that ice thicknesses  
372 measured with 2.5 and 5 MHz antennas were generally (but not always) somewhat larger than those measured  
373 with higher frequency antennas. The ice thicknesses measured with 2.5 and 5 MHz antennas were on average 8.0  
374 m (6.9 m SD; n=31) and 3.6 m (4.8 m SD; n=136) greater, respectively, than those measured with the 25–500 MHz  
375 antennas. It is unclear exactly why these differences occur. Although a systematic bias is unfortunate, the observed  
376 differences are well below the vertical resolution (evaluated conservatively as  $\frac{1}{2}$  wavelength,  $\lambda$ ) of both the 2.5 MHz  
377 (33.6 m) and 5 MHz (16.8 m) antennas, as well as the total calculated measurement uncertainty described below.

378

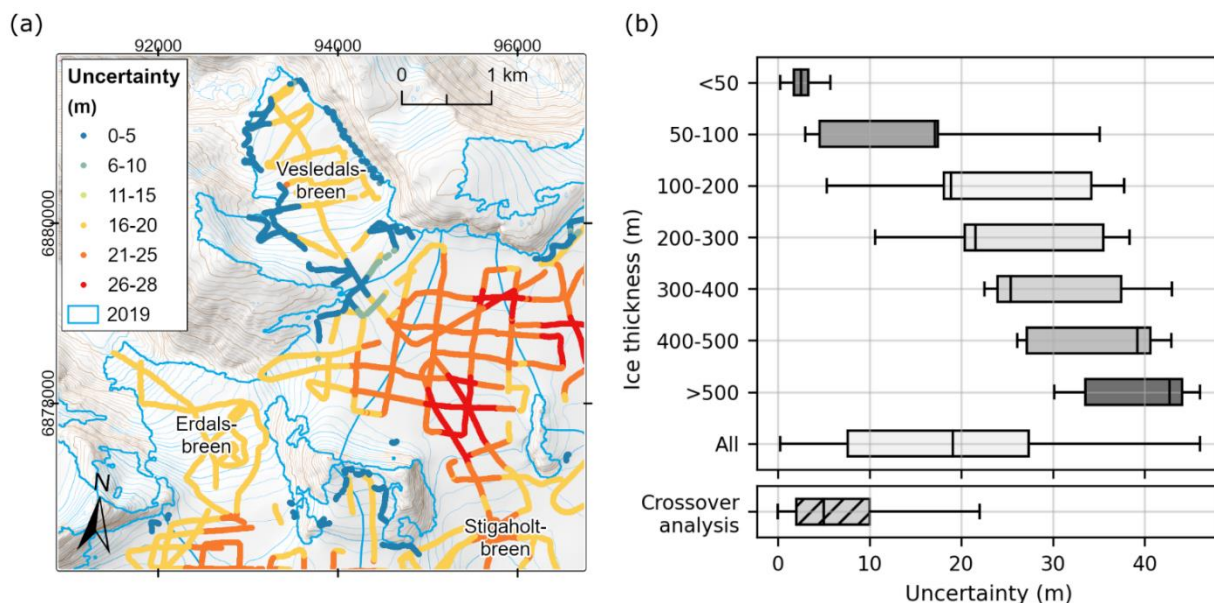


379 To evaluate the performance of the ~~new~~ 5 MHz helicopter system, we compared discrepancies between ice  
380 thicknesses measured at intersecting airborne and ground-based profiles. We found an MD of 7.2 m (4.6 m SD;  
381 n=56) between airborne and ground-based ice thickness measurements, which is comparable to values found for  
382 all ground-based and crossing 5 MHz profiles (MD of 6.5 m and a 5.0 m SD; n=705). It is worth noting that helicopter  
383 measurements along several outlet glaciers and at steep ice falls were conducted along centreline profiles, where  
384 off-nadir reflectors may affect the results (Fig. 1c). This could result in an underestimation of ice thickness in these  
385 regions. Where measurements along cross profiles suggested that the centreline values were unreliable, the latter  
386 were removed from the dataset. However, in most cases centreline values compared well with measurements  
387 along cross profiles and were largely included in the dataset.

388  
389 As a crossover analysis does not encompass all potential uncertainties associated with ice thickness  
390 measurements, it is generally considered to only provide a rough approximation of uncertainty (Lapazaran et al.,  
391 2016). Consequently, we calculated the total measurement uncertainty for each ice thickness observation using  
392 the method described by Lapazaran et al. (2016), which is based on the root-sum-of-squares of both uncertainties  
393 in the ice thickness measurements and the measurement position. Using this approach, we included uncertainties  
394 related to the radio-wave velocity, which we assumed to be 5 %, as recommended by Lapazaran et al. (2016) when  
395 the same velocity is applied in both accumulation and ablation areas. In addition, our uncertainty calculations  
396 considered the signal resolution ( $\lambda/2$ ) and positioning uncertainty. The latter was accounted for by calculating the  
397 largest measured ice thickness difference within a circle, with the radius determined by the respective GNSS  
398 uncertainty. Using this approach, total ice thickness uncertainties were primarily controlled by antenna frequency  
399 and ice thickness because of their influences on vertical resolution and the uncertainty caused by the constant  
400 radio-wave velocity, respectively (Fig. ~~76~~ and Fig. ~~B4C1~~).

401  
402 The calculated combined uncertainties of the ice thickness measurements amounted to an average of 19.6 m for  
403 the entire dataset (SD of 12.1 m; n = 351 559), while mean ice thickness uncertainties ranged between 36.5 m (SD  
404 of 2.5 m) and 20.2 m (SD of 3.1 m) for 2.5 and 5 MHz measurements, respectively, and 1 m (SD of 0.5 m) for 450  
405 and 500 MHz measurements. The large mean uncertainty estimate calculated for most ice thickness observations  
406 was primarily a result of the conservative treatment of signal resolution and the assumed 5 % uncertainty from  
407 applying a single radio-wave velocity value to the entire ice cap despite ice cap-wide variations in snow, firn, and  
408 thermal ice conditions. The significantly larger measurement uncertainty found using the method of Lapazaran et  
409 al. (2016) compared to the crossover analysis (Fig. ~~76b~~), implies that the former approach leads to an  
410 overestimation of uncertainties associated with relatively low frequency (below ~10 MHz) ice thickness  
411 measurements, particularly in regions with thick ice. We therefore suggest that the crossover analysis and the  
412 calculated measurement uncertainty represent a lower and upper estimate, respectively, of the uncertainties

413 associated with each ice thickness observation. In the datafile compilation presented here, we include only the  
414 upper estimate of total measurement uncertainty.  
415



416

417 **Figure 76:** (a) Calculated ice thickness measurement uncertainties at Vesledalsbreen (Fig. 1). Variations in  
418 measurement uncertainties are primarily controlled by antenna frequency, with <5 m uncertainty for 500 MHz  
419 measurements, between 6 and 13 m uncertainty for 50 MHz measurements and  $\geq 14$  m for 5 MHz measurements. The  
420 largest measurement uncertainties are found in regions with thick ice, illustrating the influence of ice thickness on the  
421 uncertainty calculations. (b) Distribution of calculated absolute uncertainty in ice thickness by thickness class and for  
422 all measurements following the method described by Lapazaran et al. (2016), as well as that observed in the crossover  
423 analysis. Boxes represent the interquartile range (IQR; the spread of the middle 50 % of the data), with medians  
424 indicated by vertical lines. Whiskers extend to the highest and lowest values that are within the 1.5\*IQR limits. The  
425 background map in (a) is from the Norwegian Mapping Authority (WMS for Topografisk Norgeskart available at  
426 <https://www.geonorge.no/>) and the 2019 ~~outline~~ outlines of Jostedalbreen glacier units ~~is~~are from Andreassen et al.  
427 (2022). The coordinate system is UTM 33N, datum ETRS\_1989.

### 428 3.5 Description of datafile compilation

429 The ice thickness point values from Jostedalbreen were compiled in a format similar to that of the Glacier  
430 Thickness Database (GlaThiDa Consortium, 2020; Welty et al., 2020) for straight-forward application in future  
431 studies. Data were stored in a CSV (comma-separated values) file with attributes describing the data (Table 2),  
432 and a DOI is provided for the ice thickness dataset. Consequently, the dataset follows the FAIR principles of  
433 optimised findability, accessibility, interoperability, and reusability.

434

435

**Table 2: Attributes used in the point dataset of ice thickness values on Jostedalbreen.**

Attributed field	Unit	Description
SURVEY_DATE	YYYYMMDD	Survey date
PROFILE_ID	Text	Identifier of processed radar profile
POINT_ID	Number: 1-n	Point identifier
ANTENNA_FREQUENCY	MHz	Antenna frequency of measurement
SURVEY_METHOD	Text: H, S or F	Means of transport during survey (H: Helicopter, S: Scooter, F: Foot)
GNSS_SOURCE	Number: 0 or 1	Position information (0: Radar GNSS (lowest uncertainty) and 1: External GNSS source or some degree of interpolation across minor data gaps)
POINT_LAT	DDD.DDDDDD°	Latitude of point value
POINT_LON	DDD.DDDDDD°	Longitude of point values
GNSS_ELEVATION	m a.s.l.	Surface elevation from GPR GNSS
THICKNESS	Meter	Ice thickness value
THICKNESS_UNCERTAINTY	Meter	Uncertainty in ice thickness based on Lapazaran et al. (2016)
THICKNESS_2020DTM	Meter	Ice thickness value homogenised to the 2020 DTM surface-*. Corrected for differences in surface elevation during survey years relative to the 2020 DTM.

437 \*Survey date August 2020 except for the lower part of Tunsbergdalsbreen.

438

439 Most of the attributes in the table containing ice thickness point values are self-explanatory and identical to those  
 440 in GlaThiDa. However, data entries such as SURVEY\_METHOD, GNSS\_SOURCE and THICKNESS\_2020DTM  
 441 are additional attributes to describe the Jostedalbreen data collection. In addition to the datafile containing the  
 442 complete ice thickness dataset (n = 351 559 entries), we provide a thinned-out version of this dataset (n = 35 100  
 443 entries) consisting of point values extracted randomly from the full dataset but with a minimum distance of 20 m.  
 444 The smaller dataset allows for easier plotting and analysis.

### 445 3.6 Model-based ice thickness inter- and extrapolation

446 While the dense network of GPR profiles across large parts of the ice cap provides direct local information on ice  
 447 thickness on 59 out of the 81 glacier units that make up Jostedalbreen ice cap (Fig. 1), an extrapolation to  
 448 unmeasured regions was necessary to produce grids of ice thickness and bed topography which cover the entire  
 449 Jostedalbreen. Here, we apply an approach that combines the advantages of inter- and extrapolation of point ice  
 450 thickness observations with those of iceice thickness modelling from an inversion of surface topography (Huss and  
 451 Farinotti, 2014; Grab et al., 2021). The basis of this approach is an ice thickness model originally developed for

452 global-scale applications (Huss and Farinotti, 2012). The model was used in the Ice Thickness Model  
453 Intercomparison eXperiment (ITMIX and ITMIX2, Farinotti et al., 2017, 2021) and performed well in estimations of  
454 ice thickness distribution and bed topography—in comparison to a wide range of other approaches. This was the  
455 case both if no nearby ice thickness measurements were available, and when such observations were integrated  
456 for constraining model parameters.

457  
458 The general concept of the model for glaciers without measurements is to derive local ice thickness from surface  
459 characteristics. ~~#The model~~ relies on glacier surface hypsometry of all individual glacier units of Jostedalsbreen,  
460 discretised into 10 m elevation bands. Variations in the valley shape and the basal shear stress along each outlet  
461 glacier's longitudinal profile, as well as an estimated ~~longitudinal trend in constant~~ basal sliding fraction of 0.5 (e.g.,  
462 Huss and Farinotti, 2012), are taken into account. Ice volume fluxes are computed along a longitudinal profile based  
463 on calibrated mass balance gradients. Subsequently, ice thickness is calculated by inverting the flow law for ice  
464 (Glen, 1955-), thus assuming parallel flow consistent with the shallow-ice approximation. Resulting averages of  
465 elevation-band ice thickness are then ~~extrapolated~~interpolated to a regular grid by considering both local surface  
466 slope and distance from the glacier margin, excluding ice divides (for details see Huss and Farinotti, 2012). For  
467 glacier units with ice thickness measurements (i.e., the vast majority of Jostedalsbreen) the modelled ice thickness  
468 is first optimised to fit the measurements and then only used in unmeasured regions along with all measured point  
469 thicknesses in an inverse-distance interpolation scheme (see details below). Our approach provides a spatially  
470 complete ice thickness and bedrock grid that agrees with all thickness observations. We decided to use this  
471 methodology rather than approaches based on assimilating the ice flux divergence (e.g., Fürst et al., 2017;  
472 Morlighem et al., 2017), as we attribute the highest weight to fitting the comprehensive set of measurements that  
473 are at the core of the present study.

474  
475 Before initialising the model-based ice thickness inter- and extrapolation, we harmonised the spacing of the  
476 acquired profiles by taking the average of all homogenised ice thickness point data contained within the same 10  
477 x 10 m cell of the DTM10. The ice thickness point dataset and the outline of Jostedalsbreen both serve as important  
478 input when computing spatially distributed ice thickness. As glacier outline, we used the national glacier inventory  
479 which relies on Sentinel-2 images taken on 27 August 2019 (Andreassen et al., 2022). In this dataset,  
480 Jostedalsbreen is divided into glacier units from topographic observations on ice divides. The inventory was derived  
481 using a standard semi-automatic method and checked against orthophotos and Sentinel composites from 2017  
482 and 2019, respectively, with manual edits to correct for areas in shadow, with debris-cover, and lake outlines. The  
483 uncertainty in the outlines of the final product was estimated to be within half a pixel ( $\pm 5$  m).

485 Our dataset of distributed ice thickness for all Jostedalsbreen was produced by optimising modelled ice thickness  
486 to local ice thickness observations for each individual glacier unit, following a three-step procedure that consisted  
487 of (i) model optimisation, (ii) spatial bias-correction of modelled thicknesses, and (iii) spatial ~~interpolation~~inter- and  
488 extrapolation relying on point values of thickness and bias-corrected model results for regions that are not covered  
489 by GPR surveys.

490  
491 In step (i), we optimised the apparent mass-balance gradient (Farinotti et al., ~~2009~~2009) for the ablation and  
492 accumulation area, assuming a constant ratio of 1.8 between the gradients, in an automatic procedure to minimise  
493 the average misfit between modelled ice thickness and the available observations for each of the 59 outlet glaciers  
494 with ice thickness measurements. ~~The apparent mass balance was then computed based on two linear elevation~~  
495 ~~gradients, one for~~ To close the ~~ablation area and one for the accumulation area, assuming mass budget, we~~  
496 prescribed a balanced mass budget for the entire glacier unit. (see Farinotti et al., 2009). The resulting apparent  
497 mass balance distribution was then used to compute ice volume fluxes from the top to the bottom of each glacier  
498 unit, and to infer modelled ice thickness distribution ~~as in Andreassen et al. (2015)~~.

499  
500 In step (ii), the modelled ice thickness distribution from step (i) was bias-corrected using ice thickness point values.  
501 First, relative differences between modelled and measured point ice thickness distributions were evaluated. These  
502 differences were then spatially inter- and extrapolated based on an inverse-distance weighting scheme ~~that results~~  
503 in a smooth field over the entire glacier and allows extracting large-scale spatial variations in misfits. This relative  
504 spatial ice thickness correction field was then superimposed on the modelled ice thickness distribution, resulting in  
505 a bias-corrected model-based ice thickness distribution that accounts for the differences between observed and  
506 modelled ice thickness at a spatially distributed scale. ~~Nevertheless, this ice thickness distribution will not exactly~~  
507 match all GPR-derived point values of thickness.

508  
509 In the final step (iii), we spatially interpolated the ice thickness distribution based on (1) all available ice thickness  
510 observations, (2) the model results adjusted in steps (i) and (ii) in regions that were not covered by direct  
511 measurements (buffered in a distance of 100–200 m around available observations depending on outlet glacier  
512 size), and (3) the condition of zero ice thickness on the glacier margin, except for ice divides. The combined dataset  
513 of measured and modelled point ice thickness were directly interpolated using an inverse-distance weighting  
514 scheme to achieve a full coverage for each glacier at a 10 m grid spacing.

515  
516 The ice thickness at ice divides was obtained from ~~model~~interpolated results ~~off~~ neighbouring outlet  
517 glaciersglacier units, and then also entered the interpolation. Estimates for ice thickness at ice divides is, thus,  
518 given by nearby direct measurements or model results. Furthermore, for a few situations with poorly constrained

519 ice divide thicknesses a set of individually estimated ~~thicknesses on ice divides based on local knowledge and~~  
520 ~~direct interpolation of nearby GPR profiles point thicknesses~~ was included to increase the robustness of spatially  
521 complete ice thickness ~~estimates at ice divides and bedrock grid~~. These estimated point ice thicknesses were  
522 acquired from a direct interpolation of nearby GPR profiles in ArcGIS pro, that involved (1) a 20 m grid spline  
523 interpolation (8 sector search radius) of ice thickness measurements and subsequent extraction of 10 m ice  
524 thickness contour lines, (2) smoothing of contour lines (50 m smoothing tolerance), and (3) a Topo to Raster  
525 interpolation from smoothed contour lines. Repeating the complete procedure several times ensured convergence  
526 and thus consistency of thicknesses on both sides of the ice divides, thus avoiding thickness steps at ice divides  
527 even though glacier units were treated separately in our approach. For glacier units without GPR measurements,  
528 the ice thickness model was run using average calibrated parameters of the apparent mass-balance gradient from  
529 all outlet glaciers with direct observations. This direct modelling of ice thickness, however, was only relevant for  
530 small and mostly thin glacier units within Jostedalsbreen, and account for just 1.9 % of the total inferred volume of  
531 the ice cap. We finally combined all ~~results of extrapolated~~ resulting ice ~~thickness~~ thicknesses from the 81 glacier  
532 units contained in Jostedalsbreen into a complete coverage with a spatial resolution of 10 x 10 m.

### 533 **3.7 Bed topography and potential future lakes**

534 Bed topography was obtained by subtracting distributed ice thickness from the DTM10 ice surface elevation. The  
535 resulting grid of bed topography was then smoothed with a spatial filter of 20–50–100 m (depending on glacier  
536 basin area) to remove remaining discontinuities at ice divides, as well as unrealistic small-scale variability in  
537 calculated bed topography that cannot be inferred with the applied methodology and will originate from surface  
538 features. Depressions in the bed topography might act as potential future lakes after complete disappearance of  
539 the ice cover. Even though the uncertainty in detecting the extent and volume of such depressions is large, we  
540 derived a map of potential lake area and depth from the map of subglacial bed topography. This was achieved by  
541 using a sink fill algorithm that detected depressions, after which the depth and volume of each depression was  
542 determined by artificially filling the depression until they overflow. This resulted in an inventory of individual potential  
543 glacier lakes, including the relevant attributes, such as their elevation, area, volume, or maximum depth.

### 544 **3.8 Uncertainties in inter- and extrapolated ice thickness**

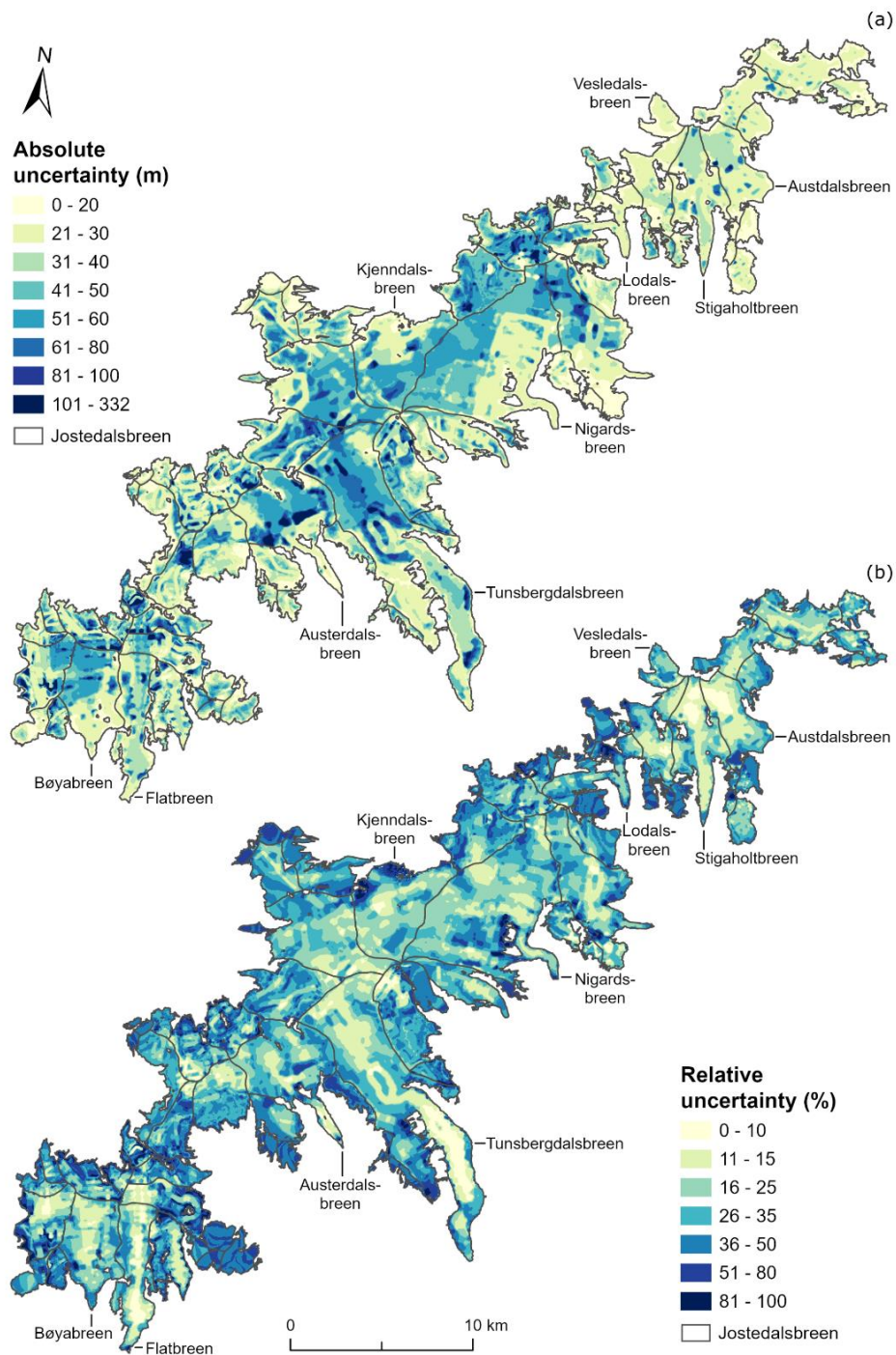
545 The uncertainty in inter- and extrapolated ice thickness is composed of two elements: (1) the uncertainty in  
546 measured ice thickness, and (2) the uncertainty induced when extrapolating point ice thickness across the entire  
547 ice cap supported by the model-based approach. These two elements of uncertainty are estimated separately with

548 ~~separate experiments~~, and are then propagated through the methodology described above to derive a spatially  
549 distributed uncertainty map for the entire ice cap.

550  
551 As described in section 3.4, the uncertainty associated with each point value of ice thickness was calculated  
552 following Laparazan et al. (2016). We conservatively assume all uncertainties across the entire ice cap to be  
553 correlated and generate a dataset with maximum ~~observed thickness~~ and minimum observed ice thickness  
554 according to the above uncertainties. Based on these two datasets, we repeated the complete approach described  
555 in section 3.6 using each of these datasets. ~~Taking two additional experiments were conducted to assess the mean~~  
556 ~~local deviation uncertainty caused by extrapolating observations to unmeasured regions. Relevant parameters of~~  
557 ~~the results from ice thickness model were set to the~~ maximum or the minimum of conservative, but physically  
558 meaningful, ranges. This was performed for (1) the viscosity of ice, (2) the assumed fraction of basal sliding, and  
559 (3) the apparent mass balance gradients. In both experiments, the reference dataset of point ice thickness  
560 distribution values was used for calibration (see Section 3.6), such that the resulting thickness grids differ mostly in  
561 regions where ice thickness is solely inferred ~~with the reference approach, we computed a spatially distributed~~  
562 ~~uncertainty estimate due to measurement uncertainty by the model.~~

563  
564 ~~To assess the uncertainty caused by extrapolating observations to unmeasured regions, we performed a suite of~~  
565 ~~sensitivity experiments by varying different parameters of the model-based approach within conservatively set, but~~  
566 ~~physically meaningful, ranges. This was performed for the viscosity of ice, the assumed fraction of basal sliding,~~  
567 ~~and the apparent mass balance gradients. In each experiment, the reference dataset of point ice thickness values~~  
568 ~~was used for calibration, such that the resulting ice thickness grids differ mostly in regions where ice thickness is~~  
569 ~~solely inferred by the model.~~

570  
571 Finally, we combined the ~~local~~ offset from the reference ice thickness distribution at all grid cells for ~~all the four~~  
572 ~~experiments~~ described above (two for measurement uncertainty, two for model uncertainty) based on the root-sum-  
573 of-squares ~~resulting. This results~~ in an absolute and a relative uncertainty grid ~~(Fig. 8).~~ Local uncertainties were  
574 bounded to not exceed the grid cell's reference ice thickness which occurred in a few instances close to glacier  
575 margins. ~~Typically, this grid indicates small uncertainties close to the GPR profiles and larger uncertainties in~~  
576 ~~regions where the result is based on ice thickness modelling. Overall, we find a mean uncertainty in local ice~~  
577 ~~thickness of 36 m (30%), where regions with thick ice are characterized by high absolute but low relative thickness~~  
578 ~~uncertainties, and vice versa for regions with thin ice (Fig. 8).~~



580  
 581 **Figure 8: (a) Absolute and (b) relative uncertainty for distributed ice thickness on Jostedalsglaciären. The two figures**  
 582 **illustrate that the largest absolute uncertainties appear in regions with thick ice and away from GPR profiles, while the**



583 ~~largest relative uncertainties are found in the thin ice marginal regions. The 2019 outline of Jostedalsbreen glacier~~  
584 ~~units is from Andreassen et al. (2022).~~

586 To assess the relevance of additionally set thickness points along ice divides used to better constrain the thickness  
587 inter- and extrapolation in these regions (see Section 3.6.) we performed an experiment where these supporting  
588 points were removed. We find that the effect on the inferred total ice volume of Jostedalsbreen. The two figures  
589 illustrate that the largest is minimal (-1.1%), and that local thicknesses are affected by 1.2 m on average (median  
590 absolute difference).

591  
592 We note that beyond the uncertainties appear in regions estimated above, our dataset of gridded thickness and  
593 bedrock for entire Jostedalsbreen comes with thick ice and awaysome limitations that should be considered  
594 regarding the usage: We intentionally rely on a statistical inter- and extrapolation of measured point thickness here  
595 and supplement this data with results from GPR profiles, while the largest relative uncertainties are found modelling  
596 in the thin ice marginal unmeasured regions. The 2019 outline of Jostedalsbreen glacier units is from Andreassen  
597 et al. This might result in inconsistencies with the application of a three-dimensional ice flow model as our product  
598 is not optimised to correspond to a smooth flux-divergence field. Nevertheless, we argue that in the frame of the  
599 present publication, whose main emphasis is on measured ice thickness, we strive to optimally make use of these  
600 observations and to attribute them with the highest weight in our gridded dataset. This also drives the decision to  
601 post our results on a 10 m grid, which may imply an exaggerated accuracy for regions without direct measurements  
602 but allows resampling to coarser resolutions, depending on the specific application.

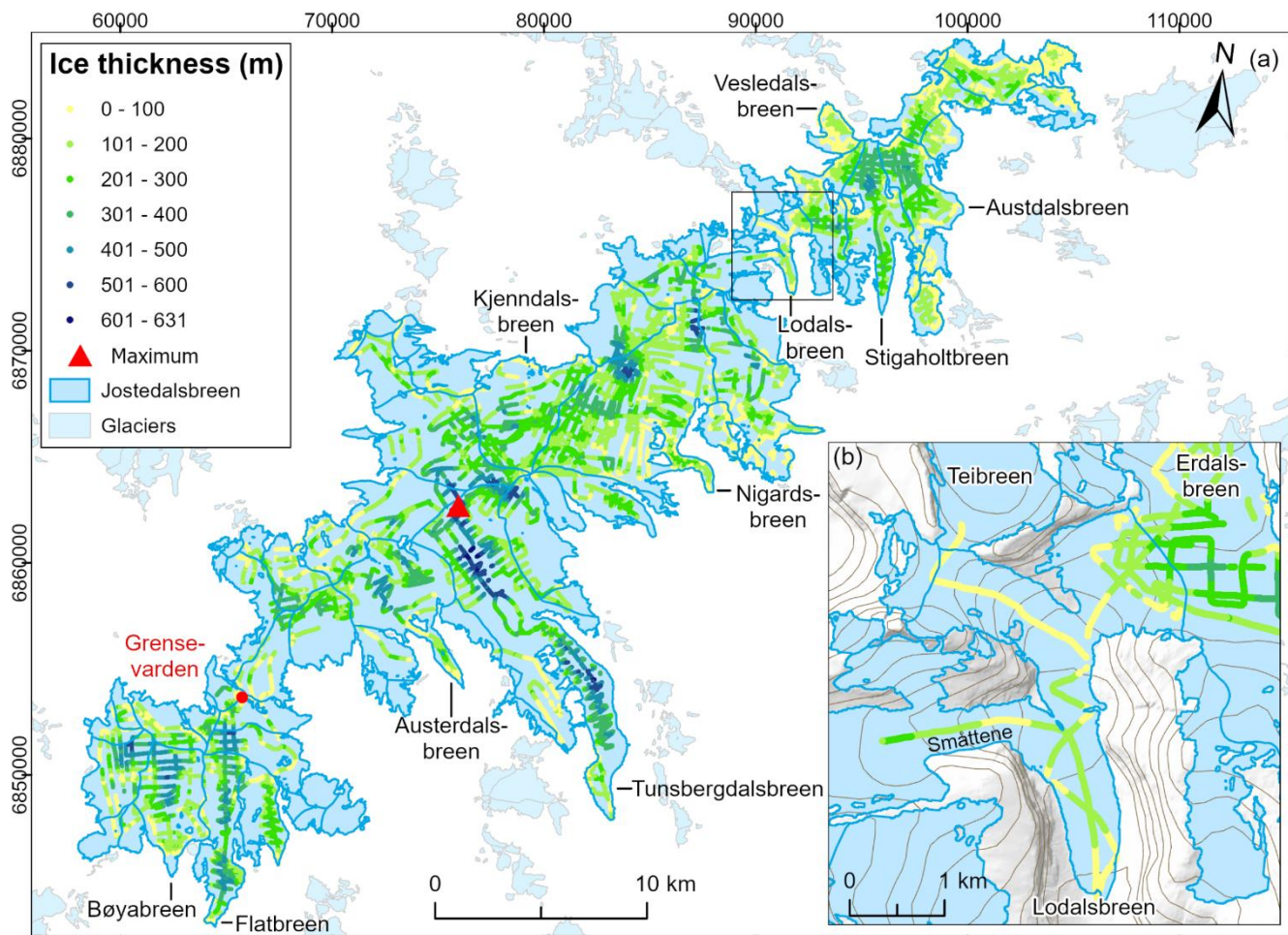
## 603 **4 Results**

### 604 **4.1 Measurements of ice thickness**

605 The dataset presented here provides ice thickness point values for 59 of the 81 glacier units that constitute the  
606 Jostedalsbreen 2019 inventory. These 59 glaciers cover 437 km<sup>2</sup>, or 95 % of the total area of the ice cap (458 km<sup>2</sup>  
607 in 2019). All parts of Jostedalsbreen are now less than 900 m from a point of known ice thickness (measurement  
608 or glacier outline), while distances to a known point are less than 300 m for 90 % of the ice cap and less than 100  
609 m for 49 % of the ice cap. A maximum ice thickness of 631 m (or 628 m when referring to 2020 DTM) was measured  
610 in the upper accumulation area of Tunsbergdalsbreen, which is the largest outlet glacier of Jostedalsbreen and  
611 located in the central part of the ice cap (Fig. 4 and 97). In Jostedalsbreen South and North, ice thickness reaches  
612 maximum values of ~520 and ~430 m, respectively. In general, the thickest ice at Jostedalsbreen is found in the  
613 flattest areas of the ice cap, while thinner ice of less than 100 m thickness covers protruding hills. In the northern

614 parts, the highest mountains in the landscape surrounding Stigaholtbreen (Fig. 76a and 97) are already partially  
615 ice-free, giving the ice cap a more disjointed appearance in this region.

616  
617 Along the south-eastern margin of Jostedalbreen, large outlet glaciers flow far into the valleys below. Particularly  
618 thick ice is found along the three glacier tongues of Tunsbergdalsbreen (up to ~615 m), Flatbreen (up to ~435 m)  
619 and Stigaholtbreen (up to ~320 m) (Fig. 97). These outlet glaciers are characterised by large accumulation areas  
620 from which ice flows relatively unrestricted from the innermost parts of the ice cap plateau and along deep glacier-  
621 carved valleys. In comparison, thinner ice is observed along outlet glaciers where ice flows from the ice cap plateau  
622 through steep ice falls. Austerdalsbreen with its two steep ice falls and low-sloping glacier tongue, represents one  
623 such example. Here, helicopter measurements along the centre flowline of the largest of the two narrow ice falls  
624 suggest that the ice is only 40–50 m thick in the steepest parts. Below the ice falls, ice thickness reaches a  
625 maximum of ~235 m. At Nigardsbreen, ice also thins to 40–50 m as it flows through the two smallest western ice  
626 falls. Here, the main flow of ice from the ice cap plateau appears to occur through the much larger northern tributary,  
627 where centre-line ice thicknesses of more than 100 m were measured in the thinnest regions. Below the three ice  
628 falls, ice thickness reaches a maximum of ~265 m before thinning towards the famous glacier front of Nigardsbreen.



632  
 633 **Figure 97:** (a) Combined ice thickness observations at Jostedalsglacier from the field campaigns in 2018, 2021, 2022  
 634 and 2023. The point of maximum thickness is marked with a red triangle. (b) Section of Lodalsbreen with 100 m surface  
 635 contours. Note that the helicopter measurements along Lodalsbreen were collected during the first test flight of the  
 636 airborne radar system, where profile locations were positioned less than ideal in relation to the valley orientation. The  
 637 background mountain shadow and 100 m contour lines in (b) are from the Norwegian Mapping Authority (WMS for  
 638 Topografisk Norgeskart available at <https://www.geonorge.no/>). The 2019 outline of Jostedalsglacier  
 639 units is are from Andreassen et al. (2022), and the coordinate system is UTM 33N, datum ETRS\_1989.

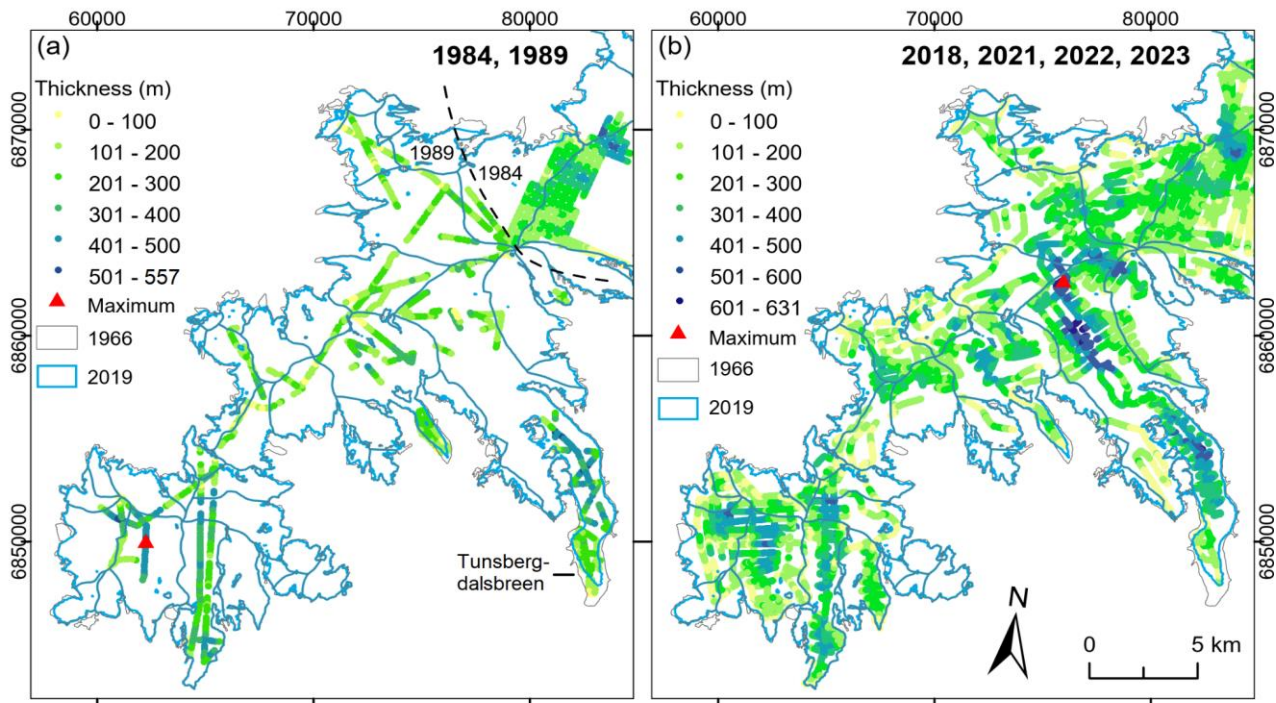
640  
 641 From the extensive measurements of ice thickness, we have identified two regions that may be particularly  
 642 vulnerable to future climate-forced changes and that have the potential to separate Jostedalsglacier into three  
 643 unconnected ice caps, North, Central, and South (Fig. 1). In the north, Lodalsbreen currently connects the  
 644 northernmost part of Jostedalsglacier with its more southern regions through three steep tributaries (Fig. 9b7b).  
 645 Helicopter measurements along the centre flowlines reveal that the ice thins to 50 m or less as it flows southwards  
 646 and into the incised valley below. Ice flowing from the western tributary is thicker, with ice thicknesses ranging  
 647 between 50 and 70 m along its thinnest sections. A study of surface elevation changes at Jostedalsglacier between

648 1966 and 2020 shows that the ice cap has experienced significant thinning in this region (Andreassen et al., 2023).  
649 This trend is likely to continue as Jostedalsbreen adjusts to warmer air temperatures. Further south on  
650 Jostedalsbreen, thin ice of less than 25 m covers the narrow stretch at Grensevarde that joins the southern part  
651 of the ice cap with its central regions (Figs. 3 and 97). Bedrock has already started protruding through the thinning  
652 ice, and the emerging rocks are likely to further accelerate the changes occurring in this part of Jostedalsbreen due  
653 to positive feedback on melting from a decreasing albedo of the surroundings. However, it is important to note that  
654 while thin ice may indicate increased vulnerability to future warming, other factors such as ice velocity and surface  
655 mass balance are important influences when considering future changes in areas with thin ice. Such considerations  
656 require ice cap-wide modelling of glacier evolution and are beyond the scope of this paper.

#### 657 **4.2 Comparison to previous ice thickness measurements at Jostedalsbreen**

658 The new comprehensive dataset of Jostedalsbreen ice thicknesses represents a significant improvement to  
659 previous measurements, both in relation to data quality and spatial coverage across the ice cap. We now have a  
660 much better understanding of ice thickness variations in the region and have also extended the maximum measured  
661 ice thickness from 600 m measured during the 1980s field campaigns (Sætrang and Wold, 1986) to the 631 m  
662 measured in 2021. Although the general ice thickness variability identified in the new measurements are also  
663 recognisable in the older datasets, distinct differences between the datasets are observed across the ice cap (Fig.  
664 8). Regions with thick ice are particularly poorly resolved in the earlier measurements, most likely due to limitations  
665 in the radar system applied during these field campaigns. While we believe that most of the discrepancies can be  
666 attributed to measurement uncertainties, evidence of glacier retreat since the measurements in 1989 is discernible  
667 in marginal regions.

668  
669



670  
 671 **Figure 8: (a) Previous ice thickness measurements collected in the southern part of Jostedalsglacier in 1984 and 1989.**  
 672 **Only the 1989 dataset is included in GlaThiDa (GlaThiDa consortium, 2020) due to large positioning uncertainties in**  
 673 **the 1984 measurements. (b) Ice thickness measurements collected during the 2018, 2021, 2022 and 2023 field seasons.**  
 674 **Locations of maximum measured ice thickness during the respective field campaigns are marked on both figures. The**  
 675 **1966 outline of Jostedalsglacier is from Paul et al. (2011) and the 2019 outlines of glacier units are from Andreassen et**  
 676 **al. (2022). The coordinate system on both figures is UTM 33N, datum ETRS 1989.**

677  
 678 Many of the previous ice thickness measurements conducted on Jostedalsglacier have considerable uncertainties  
 679 in measurement positioning and surface topography. Therefore, we limit ~~thea~~ further comparison of our  
 680 measurements to ice thickness observations on Austdalsglacier in the late 1980s, which we consider to be afflicted  
 681 with the lowest uncertainties. This older dataset was collected to evaluate future changes to Austdalsglacier due to  
 682 enhanced calving after the regulation of the proglacial lakes Austdalvatnet and Styggevatnet for hydropower  
 683 production (Hooke et al., 1989; Laumann and Wold, 1992). Ice thickness was measured in nine hot water drilled  
 684 boreholes and by GPR within an area of 600 by 1000 m, where the ice thicknesses ranged between 100 and 230  
 685 m (Fig. A1b, Sætrang and Holmqvist, 1987; Sætrang, 1988). The boreholes were drilled in September 1986 and  
 686 October 1987, while the GPR measurements used here for the assessment of uncertainties were collected in April–  
 687 May 1988 using an 8 MHz radar system. Comparisons between radar measurements and boreholes at the time  
 688 showed borehole bedrock elevations between 14 m below and 1 m above radar bed elevations. The overall

689 uncertainty of the radar bed elevations was estimated to be within 7 m based on results from a radar crossover  
690 analysis and observed uncertainties in positioning and surface elevation (Sætrang, 1988).

691

692 Two radar profiles from 2022 intersected the area also mapped by GPR in 1988. To allow for a comparison with  
693 the new ice thickness measurements, we interpolated a 5 x 5 m bed elevation grid from the 1988 GPR  
694 measurements and extracted the bed elevations at the nine boreholes and 454 locations covered by the GPR  
695 survey in 2022. On average, bed elevations measured in boreholes were 4 m lower than the interpolated grid, and  
696 the grid consequently shows a good replication of variations observed in both of the two older datasets. When  
697 comparing values from the interpolated grid and those obtained in 2022, we find that bed elevations calculated  
698 from measurements in 2022 were on average 14 m lower than those found with GPR in 1988 (i.e., 2022 ice was  
699 thicker than expected from the 1988 dataset). However, it is unclear whether this discrepancy relates to  
700 uncertainties concerning the earlier or the new measurements. In this region the 2022 measurements have a  
701 measurement uncertainty of 17–20 m (Fig. B4C1), and the observed discrepancies are consequently within the  
702 range of combined uncertainties.

### 703 **4.3 Distributed ice thickness, bed topography and potential future lakes**

704 The maps of ice thickness and bed topography (Fig. 409) allow for a coherent description of the variations in the  
705 morphology of Jostedalsbreen, also in regions that are not covered by GPR measurements. The two grids illustrate  
706 that thickest ice is found predominantly away from ice divides and in the prominent subglacial valleys of the largest  
707 outlet glaciers. By contrast, thinner ice and elevated subglacial bed topography are often associated with regions  
708 of the ice cap with high surface elevations. From the modelled ice thickness grid, we calculate an ice cap-wide  
709 mean ice thickness of 154 m  $\pm$ 22 m and a present (~2020) ice volume of 70.6  $\pm$ 10.2 km<sup>3</sup> (Table 3).

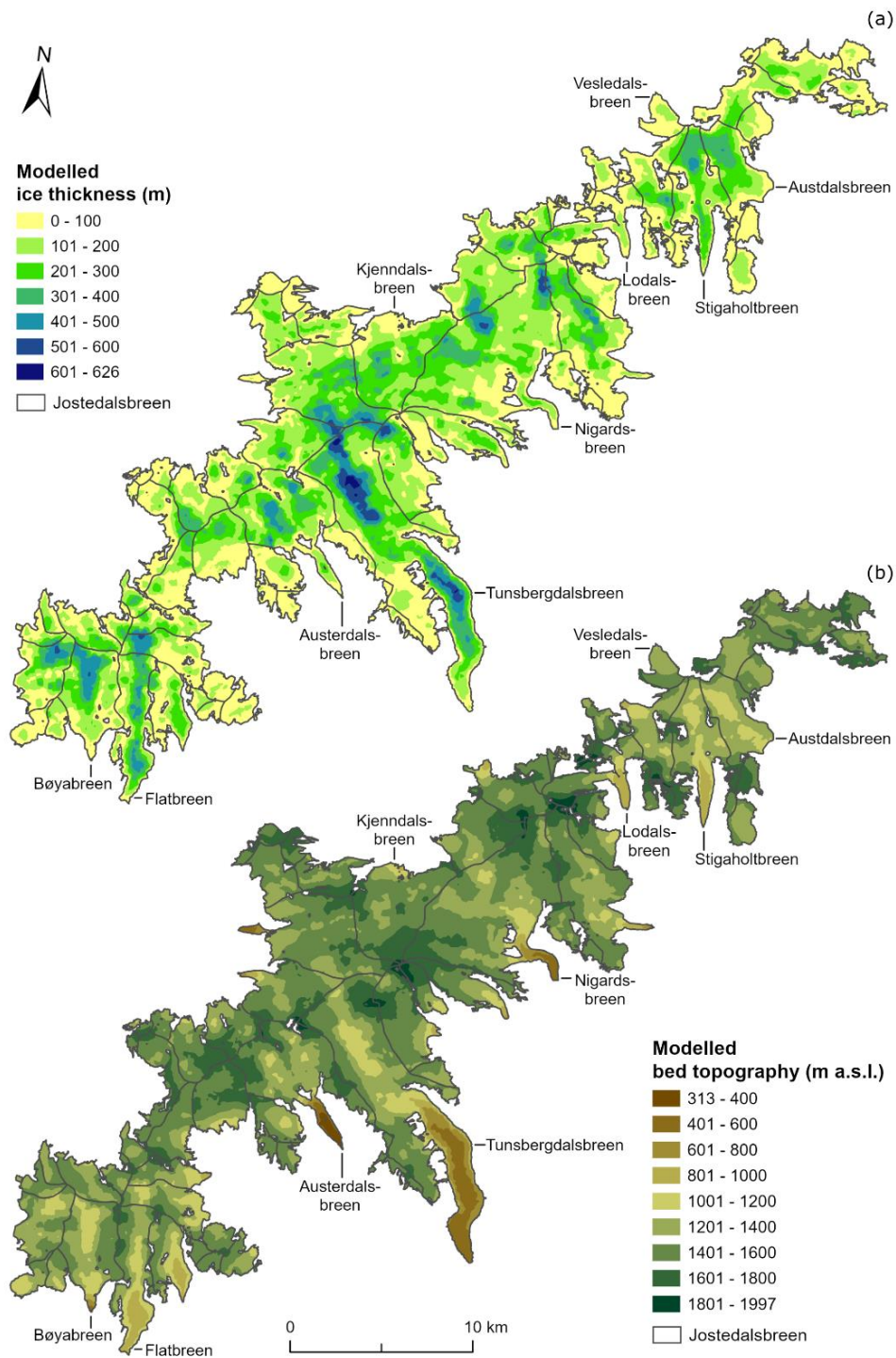
710

711 Absolute and relative uncertainty grids for the distributed ice thickness (Fig. 10) indicate that uncertainties in  
712 modelled ice thickness are typically small close to the GPR profiles and larger in regions where the result is based  
713 on ice thickness modelling. Overall, we find a mean uncertainty in local ice thickness of 36 m (30 %), where regions  
714 with thick ice are characterised by high absolute but low relative thickness uncertainties, and vice versa for regions  
715 with thin ice (Fig. 10).

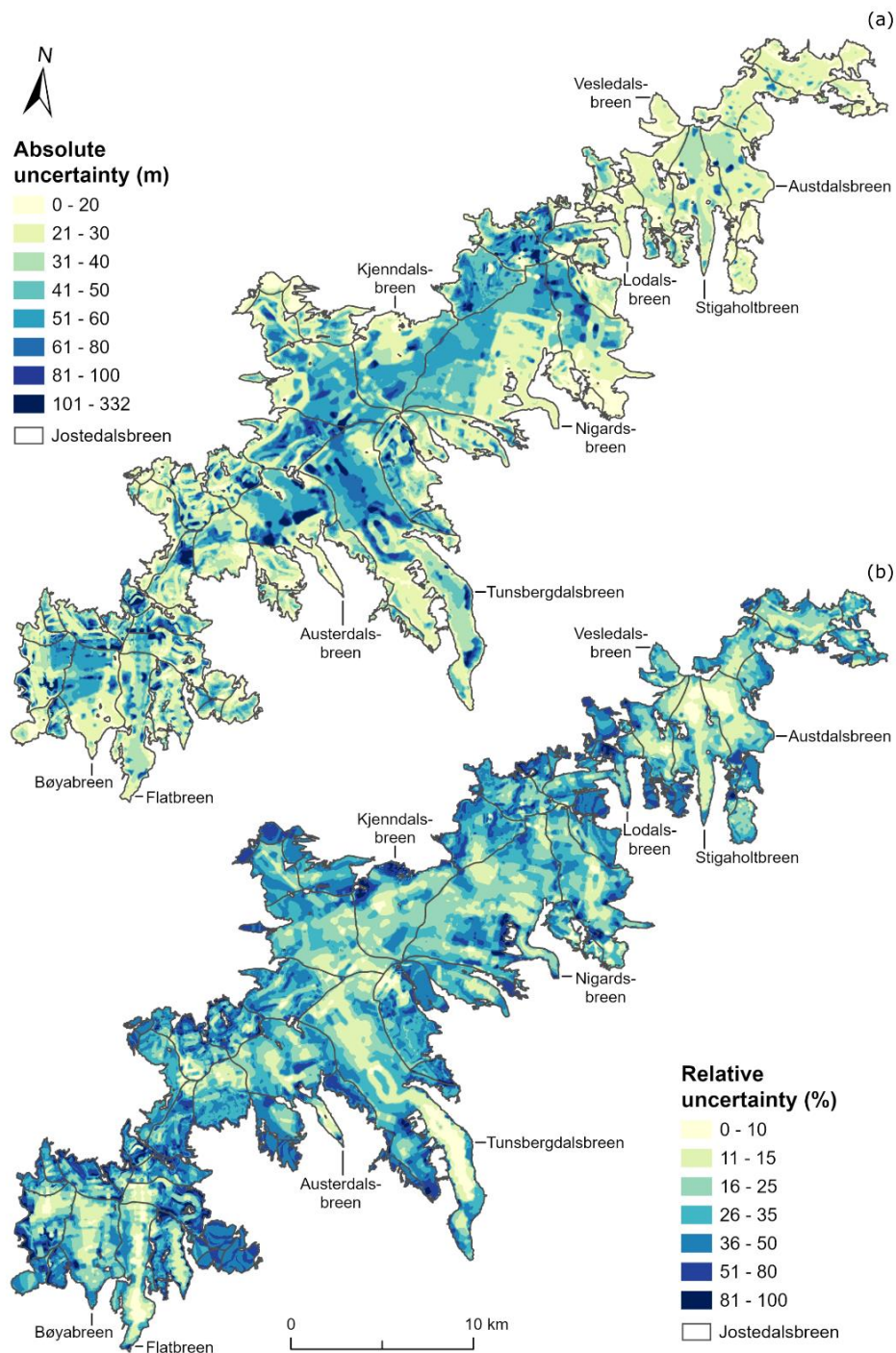
716

717

718



719  
 720 **Figure 9: (a) Modelled distributed 10 m ice thickness of Jostedalsgreen and (b) distributed 10 m bed calculated from**  
 721 **DTM10 and the modelled ice thickness distribution (Fig. 9a). The 2019 outlines of glacier units are from Andreassen et**  
 722 **al. (2022).**



723  
 724 **Figure 10: (a) Absolute and (b) relative uncertainty for distributed ice thickness on Jostedalsgreen. The two figures**  
 725 **illustrate that the largest absolute uncertainties appear in regions with thick ice and away from GPR profiles, while the**  
 726 **largest relative uncertainties are found in the thin ice marginal regions. The 2019 outlines of glacier units are from**  
 727 **Andreassen et al. (2022).**



Overall, the presented results are consistent with previous estimates ~~for~~ of the volume and ice thickness distribution Jostedalsbreen, and any smaller discrepancies are well within the uncertainty of the applied methodologies. The calculated mean ice thickness is slightly smaller than the earlier estimate of 158 m which was calculated for an interpolated region covering 65 % (310 km<sup>2</sup>) of the 2006 area (474 km<sup>2</sup>) of Jostedalsbreen (Andreassen et al., 2015). ~~Our calculated ice volume also compares well with the estimate of 72.6 km<sup>3</sup> provided by Frank and van Pelt (2024).~~ Our calculated ice volume (70.6 km<sup>3</sup>) compares well with previous volume estimates of 69.6 km<sup>3</sup> and 68.5 km<sup>3</sup> from global or regional studies provided by Farinotti et al. (2019) and Frank and van Pelt (2024) respectively, while the ice thickness model proposed by Millan et al. (2022) appears to underestimate the ice thickness at Jostedalsbreen, with a calculated volume of 56.5 km<sup>3</sup>. A comparison of our point thickness measurements with modelled values from the respective studies (Fig. 11), indicates a standard deviation of between 75 and 90 m. The mean error is small for Farinotti et al. (2019) and implies too small ice thicknesses for Millan et al. (2022) and somewhat too high ice thicknesses for Frank and van Pelt (2024).

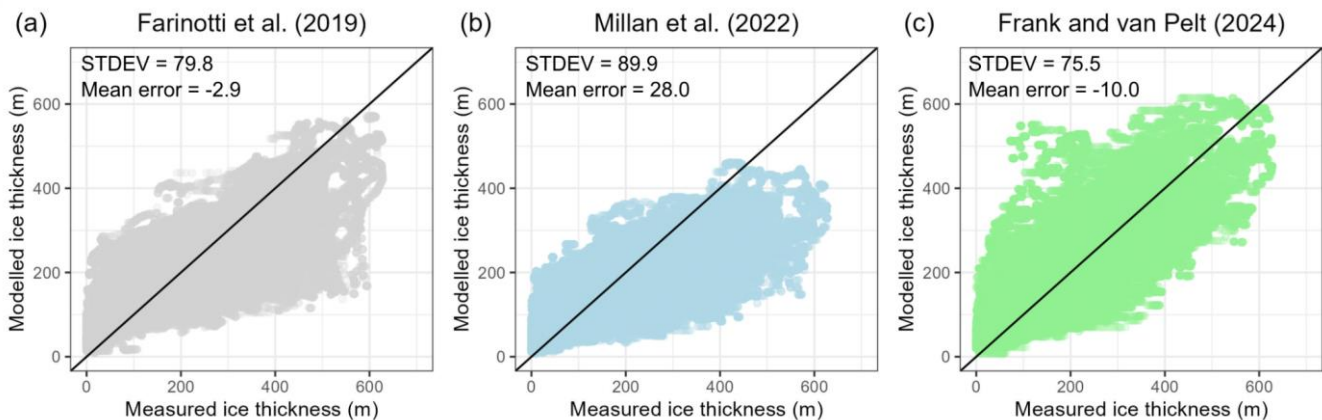
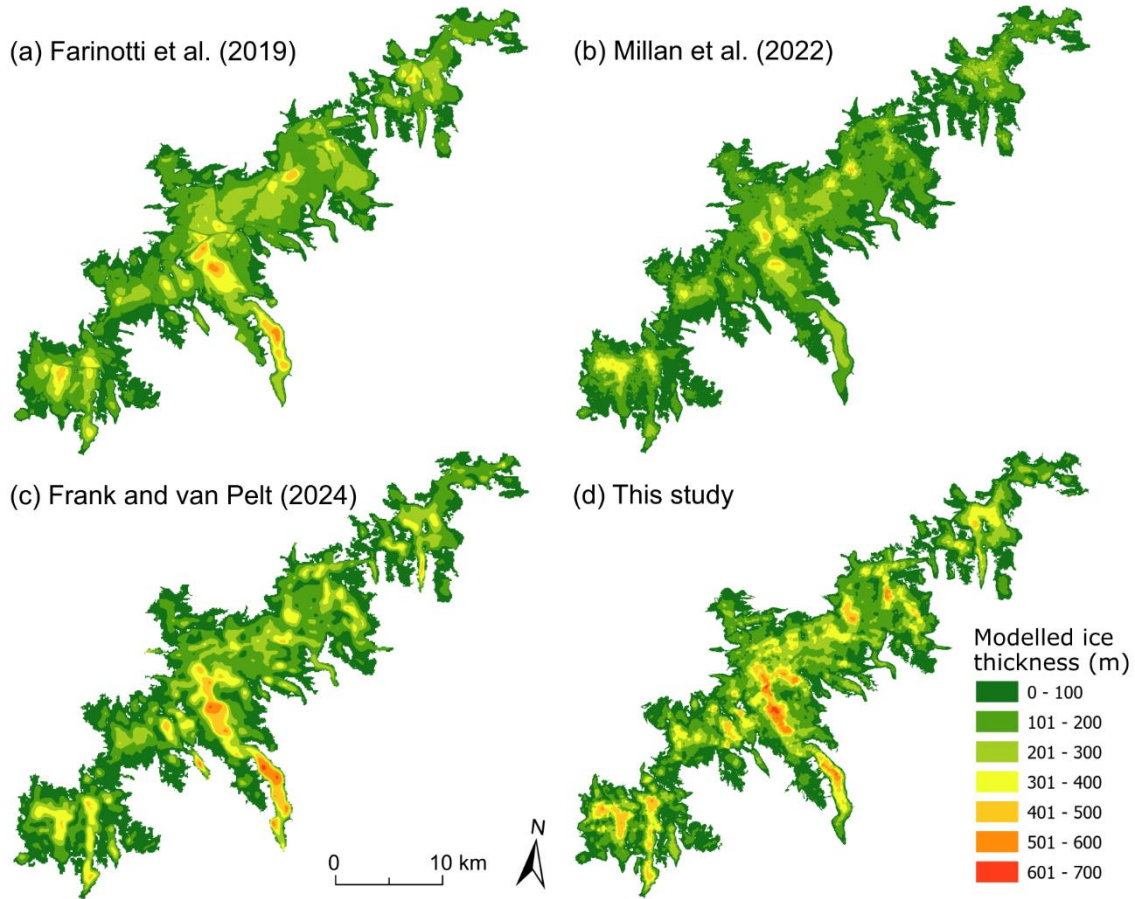


**Figure 11: Comparison of measured and modelled point ice thickness across Jostedalsbreen according to the large-scale ice thickness model datasets by (a) Farinotti et al. (2019), (b) Millan et al. (2022), and (c) Frank and van Pelt (2024). Comparisons are limited to locations within the respective model grid and calculated mean error (in meters) is negative when modelled ice thicknesses exceed measured ice thicknesses. The black line in each figure indicates the 1:1 line.**

Modelled ice thickness distribution shows that all large-scale ice thickness models capture the general pattern (Fig. 40a). ~~The 2019 outline~~12). However, the results of Farinotti et al. (2019) reveal unrealistic values along the ice divides (Fig. 12a), while the result by Millan et al. (2022) underestimates thickness both in glacial troughs and in the interior of the ice cap (Fig. 12b). The inferred thicknesses by Frank and van Pelt (2024) shows a tendency to overestimate thickness on outlet glacier tongues but in general shows an ice thickness distribution very consistent

754 with our result (Fig. 12c). Our comprehensive dataset of thickness measurements is expected to improve future  
755 regional to global-scale assessment of ice thickness distribution by supporting the calibration and validation of ice  
756 thickness models.  
757  
758



759  
760 Figure 12: Ice thickness distribution on Jostedalsbreen according to the large-scale model studies by (a) Farinotti et  
761 al. (2019), (b) Millan et al. (2022), (c) Frank and van Pelt (2024), and (d) this study.

762  
763  
764 Calculations of key numbers for selected elements of the ice cap (Table 3) show that Jostedalsbreen Central is by  
765 far the largest of the three regions when comparing area, mean ice thickness and volume. The two surrounding  
766 regions have much smaller areas and ice is generally thinner, in particularly particular in the smallest northernmost  
767 region. The ice thickness measurements presented in section 4.1 illustrate the vulnerability of Jostedalsbreen to

768 future separation into three minor ice caps. Following a future breakup, Jostedalsbreen Central would remain the  
 769 largest glacier in Norway and mainland Europe, surpassing the second largest glacier, Vestre Svartisen, which had  
 770 an area of 192.2 km<sup>2</sup> in 2019 (Andreassen et al., 2022).

771

772 **Table 3: Key numbers for the three regions and prominent outlet glaciers based on calculations from the model-based**  
 773 **grid of ice thickness for Jostedalsbreen. The bracketed values after each glacier name refer to glacier IDs from**  
 774 **Andreassen and Winsvold (2012b). Data coverage is defined as all regions which are less than 300 m from a point of**  
 775 **known ice thickness (measurements or glacier outline), with bracketed values specifying the percentage of the area**  
 776 **which are less than 100 m from a known point.**

Glacier	Area (km <sup>2</sup> )	Maximum (m)	Mean (m)	Volume (km <sup>3</sup> )	Data coverage (%)
Jostedalsbreen	458.1	626	154	70.6	90 (49)
North	69.3	432	123	8.5	99 (69)
Central	309.6	626	161	49.9	88 (45)
South	79.3	518	155	12.3	91 (47)
Lodalsbreen (2266)	8.8	329	93	0.88	98 (57)
Kjenndalsbreen (2296)	19.1	419	186	3.6	92 (50)
Nigardsbreen (2297)	41.7	572	178	7.4	98 (62)
Nigardsbreen MB* (2311, 2299 and 2297)	45.4	572	169	7.6	98 (62)
Tunsbergdalsbreen (2320)	46.2	626	233	10.8	89 (45)
Austerdalsbreen (2327)	19.4	510	191	3.7	85 (44)
Bøyabreen (2349)	13.8	501	201	2.8	99 (53)
Flatbreen/Supphellebreen (2352)	12.7	452	205	2.68	97 (58)
Austdalsbreen (2478)	10.3	402	188	1.98	100 (70)
Stigaholtbreen (2480)	12.5	432	188	2.38	99 (65)

777 \*Nigardsbreen MB refers to the mass balance glacier basin used by Andreassen et al. (2023).

778

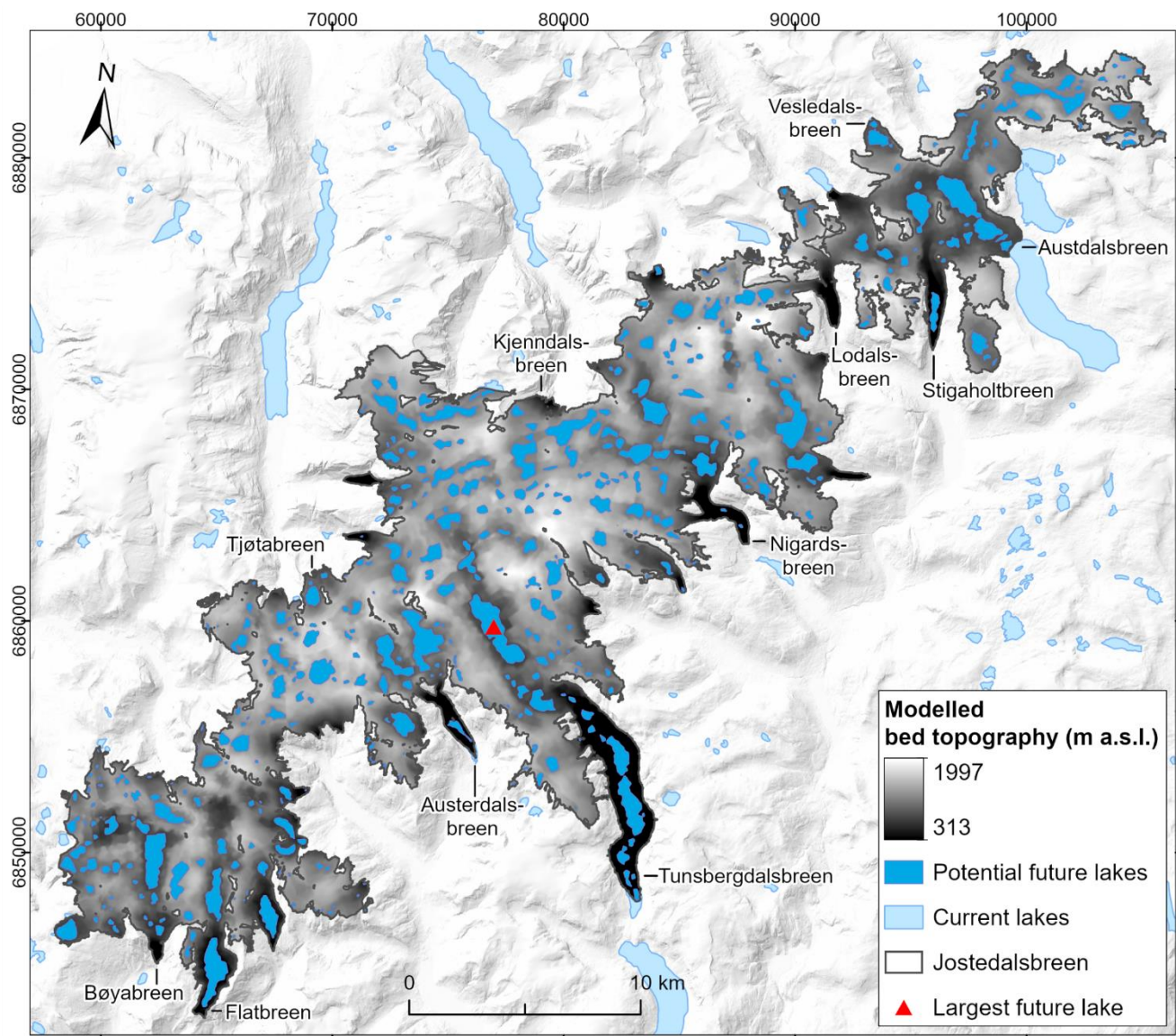
779 Beneath Jostedalsbreen we observe a versatile landscape of deep glacially incised valleys that extend to the centre  
 780 of the ice cap in some regions, and are surrounded by steep valley walls, hanging valleys and glacial over-  
 781 deepenings (Fig. 40b9b). The map of bed topography provides a glimpse of how the landscape would look ~~like~~ if  
 782 Jostedalsbreen was to completely disappear and from it we can infer possible future changes in the regional  
 783 hydrological systems. While a detailed analysis of hydrological changes in the region is outside the scope of this  
 784 study, it is worth noting that several glaciers have discrepancies between the ice divides defined by the current  
 785 surface topography of the ice cap and the hydrological catchment boundaries determined by the bed topography  
 786 in an ice-free landscape. Examples of such are Flatbreen ~~-(Supphellebreen)~~, Tunsbergdalsbreen and

787 Nigardsbreen, where the subglacial valleys appear to extend significantly beyond the current ice divides (Fig.  
788 [40b9b](#)). Other glaciers, such as at Austerdalsbreen and Lodalsbreen, have similar surface and subglacial  
789 topographical divides. Overall, it appears likely that in an ice-free landscape, upper catchment boundaries in the  
790 central and southern Jostedalsbreen regions will, in many places, be located further north and northwest than the  
791 currently more central longitudinal ice divide. In the northern parts of Jostedalsbreen, the potential extent of ice-  
792 free catchment areas appears more uncertain due to several smaller thresholds in the bed topography and  
793 limitations in data coverage across these. Consequently, we tentatively suggest that in an ice-free landscape, the  
794 topographic bed catchment at Austdalsbreen may increase substantially in size at the expense of the surrounding  
795 regions, although further analysis is required to substantiate this claim.

796

797 The distributed bed topography furthermore reveals subglacial bed depressions as likely locations for future lakes  
798 in a warming climate (Fig. [4413](#)). Our results show a multitude of potential lakes, the largest of which is 3.5 km long  
799 [and](#), has an area of 2.4 km<sup>2</sup> and is located in the inner regions of Tunsbergdalsbreen, just south of where the  
800 thickest ice was measured. Other large topographic depressions are found north of Bøyabreen and Flatbreen  
801 glacier fronts, underneath the glacier tongue of Tunsbergdalsbreen, and north-west of the calving front of  
802 Austdalsbreen. According to our estimates, a total of 14 % (65.3 km<sup>2</sup>) of the present-day glacier area of 458 km<sup>2</sup>  
803 (2019) can be covered by lakes if the entire Jostedalsbreen melts away.

804



805  
 806 **Figure 4113:** Location of current and potential future lakes calculated from the grid of subglacial bed topography at  
 807 Jostedalsglacier (Fig. 40b9b). The largest potential future lake is marked by a red triangle. The 2019 outline of  
 808 Jostedalsglacier is from Andreassen et al. (2022) and the background mountain shadow and ~~outline is~~ outlines  
 809 are from the Norwegian Mapping Authority. Outline of present-day lakes is from the Norwegian Mapping Authority  
 810 (WMS for Topografisk Norgeskart available at <https://www.geonorge.no/>) and the Norwegian Water Resources and  
 811 Energy Directorate (<https://doi.org/10.1017/jog.2022.20>). The coordinate system is UTM 33N, datum ETRS\_1989.

## 813 **5 Data availability**

814 All ice thickness observations (complete and thinned-out compilations) and maps of ice cap-wide ice thickness,  
815 combined uncertainty in ice thickness, bed topography and outlines of potential future lakes are available for  
816 download at <https://doi.org/10.58059/yhwr-rx55> which is hosted by the Norwegian Nasjonalt Vitenarkiv (Gillespie  
817 et al., 2024).

## 818 **6 Conclusions**

819 In this paper, we present a rich point dataset of high-quality ice thickness observations on Jostedalsbreen ice cap  
820 collected during GPR surveys in 2018–2023. Measurements were collected from 59 of the 81 glacier units that  
821 constitute Jostedalsbreen and 90 % of the total ice cap area is now less than 300 m from a point of known ice  
822 thickness. A maximum ice thickness of ~630 m was measured on Tunsbergdalsbreen ~~outlet glacier~~ in the central  
823 part of the ice cap. This measurement exceeds the 600 m maximum thickness previously measured on  
824 Jostedalsbreen (Sætrang and Wold, 1986; Andreassen et al., 2015). Smaller maximum ice thicknesses of ~520 m  
825 and ~430 m were measured in the southern and northern parts of the ice cap, respectively. Using this new dataset  
826 of ice thickness values, we produce model-based grids of distributed ice thickness and bed topography that allow  
827 for a coherent description of ice thickness variations and subglacial morphology over the entire Jostedalsbreen, as  
828 well as calculations of key figures for the ice cap. We find that Jostedalsbreen has a mean thickness of 154 m  $\pm$ 22  
829 m and a present (~2020) ice volume of 70.6  $\pm$ 10.2 km<sup>3</sup>. Together, the ice thickness measurements and distributed  
830 datasets provide exceptional new details about the geometry and bed topography of Jostedalsbreen, revealing  
831 vulnerabilities to future ice cap fragmentation and possible changes in the hydrological systems with climate  
832 warming. These datasets will ~~form the basis~~ of particular value to future climate change impact studies ~~of climate-~~  
833 ~~induced changes~~ in the Jostedalsbreen region, which are of high importance to local stakeholders such as farmers,  
834 tourist operators and hydropower companies.

## 835 **Author contributions**

836 MKG, JCY, and LMA designed the study. MKG led the data collection of ice thickness measurements and MKG,  
837 SDV, KHS, JA, JB, JMC, HE, BK, EL, MM, KM, SDN, TOR, EWNS and KØ carried out the fieldwork. MKG  
838 subsequently processed and interpreted the ice thickness data. MH ran the model-based extrapolation of ice  
839 thickness measurements and prepared all distributed datasets while MKG, LMA and KHS produced the figures.  
840 MKG, LMA and MH prepared the manuscript with contributions from all co-authors. JCY was the principal  
841 investigator of the JOSTICE project.

842

## 843 **Acknowledgements**

844 We would like to express our sincere gratitude to all who have contributed to the planning and implementation of  
845 the comprehensive and challenging fieldwork that was required to adequately map ice thickness across  
846 Jostedalsbreen. Especially, we would like to thank [Marthe Gjerde, Henning Åkesson and](#) Ingebjørg Haugland for  
847 assisting during the 2021 field campaign and Jostedalsbreen National Park, Nigardsbreen Nature Reserve,  
848 Breheimen National Park and the municipalities of Luster, Stryn, Sogndal, Sunnfjord and Skjåk who all granted  
849 permissions for the fieldwork. We would also like to thank Airlift AS who provided logistical support during both  
850 ground-based and airborne radar surveys. Steinmannen and Statkraft-hytta mountain huts, both owned by  
851 Statkraft, generously accommodated us during the fieldwork and snowmobiles were provided by Vang Auto-  
852 Service AS, Luster Red Cross mountain rescue group and Statkraft. Lastly, we thank Statkraft for advising on  
853 weather conditions and NVE for their local avalanche forecasting.

## 854 **Competing interests**

855 All co-authors other than EL declare that they have no conflict of interest. EL works for the hydropower company  
856 Statkraft, and Statkraft has an interest in the hydropower production at Austdalsbreen. Statkraft did not in any way  
857 influence the research objectives, data collection, analysis or interpretations of data presented in this paper.

## 858 **Financial support**

859 This study is a contribution to the JOSTICE project funded by the Norwegian Research Council (RCN grant  
860 #302458). In addition, the 2023 airborne survey was supported by funding from UH-nett Vest.

## 861 **References**

- 862 Andreassen, Elvehøy, H., Kjøllmoen, B., Engeset, R. V. and Haakensen, N.: Glacier mass balance and length  
863 variation in Norway, *Ann. Glaciol.*, 42, 317–325, 10.3189/172756405781812826, 2005.
- 864
- 865 Andreassen, L. M., Melvold, K., Nordli, Ø., Nordli, Ø., and Rasmussen, A.: Langfjordjøkelen, a rapidly shrinking  
866 glacier in northern Norway, *J. Glaciol.*, 58, 581–593, 10.3189/2012JoG11J014, 2012a.
- 867
- 868 Andreassen, L. M. and Winsvold, S. H. (eds), Paul, F. and Hausberg, J. E.: Inventory of Norwegian Glaciers, NVE  
869 report 38-2012. Norwegian Water Resources and Energy Directorate, Oslo, Norway, 2012b.
- 870
- 871 Andreassen, L. M., Elvehøy, H., Huss, M., Melvold, K., and Winsvold, S. H.: Ice thickness measurements and  
872 volume estimates for glaciers in Norway, *J. Glaciol.*, 61, 763–775, 10.3189/2015JoG14J161, 2015.
- 873

874 Andreassen, L. M., Nagy, T., Kjølmoen, B., and Leigh, J. R.: An inventory of Norway's glaciers and ice-marginal  
875 lakes from 2018–19 Sentinel-2 data, *J. Glaciol.*, 68, [1085–1106](#), [10.1017/jog.2022.20](#), 2022.

876

877 Andreassen, L. M., Carrivick, J. L., Elvehøy, H., Kjølmoen, B., Robson, B. A., and Sjrursen, K. H.: Spatio-temporal  
878 variability in geometry and geodetic mass balance of Jostedalsbreen ice cap, Norway, *Ann. Glaciol.*, 1–18,  
879 [10.1017/aog.2023.70](#), 2023.

880

881 Binder, D., Brückl, E., Roch, K. H., Behm, M., Schöner, W., and Hynek, B.: Determination of total ice volume and  
882 ice-thickness distribution of two glaciers in the Hohe Tauern region, Eastern Alps, from GPR data, *Ann. Glaciol.*,  
883 50, 71–79, 2009.

884

885 Bolibar, J., Rabatel, A., Gouttevin, I., Zekollari, H., and Galiez, C.: Nonlinear sensitivity of glacier mass balance to  
886 future climate change unveiled by deep learning, *Nat. Commun.*, 13, 409, 2022.

887

888 Carrivick, J. L., Andreassen, L. M., Nesje, A., and Yde, J. C.: A reconstruction of Jostedalsbreen during the Little  
889 Ice Age and geometric changes to outlet glaciers since then, *Quat. Sci. Rev.*, 284, 107501,  
890 <https://doi.org/10.1016/j.quascirev.2022.107501>, 2022.

891

892 Dowdeswell, J. A. and Evans, S.: Investigations of the form and flow of ice sheets and glaciers using radio-echo  
893 sounding, *Rep. Prog. Phys.*, 67, 1821, [10.1088/0034-4885/67/10/R03](#), 2004.

894

895 Engen, S. H., Gjerde, M., Scheiber, T., Seier, G., Elvehøy, H., Abermann, J., Nesje, A., Winkler, S., Hualand, K.  
896 F., Rüter, D. C., Maschler, A., Robson, B. A., and Yde, J. C.: Investigation of the 2010 rock avalanche onto the  
897 regenerated glacier Brenndalsbreen, Norway, [Submitted to Landslides, \(accepted for publication\)-21, 2051–2072,](#)  
898 [10.1007/s10346-024-02275-z, 2024.](#)

899

900 Engeset, R. V., Jackson, M., and Schuler, T. V.: Analysis of the first jökulhlaup at Blåmannsisen, northern Norway,  
901 and implications for future events, *Ann. Glaciol.*, 42, 35–41, [10.3189/172756405781812600](#), 2005.

902

903 Farinotti, D., Huss, M., Bauder, A., Funk, M., and Truffer, M.: A method to estimate the ice volume and ice-thickness  
904 distribution of alpine glaciers, *J. Glaciol.*, 55, 422–430, 2009.

905

906 Farinotti, D., Brinkerhoff, D. J., Clarke, G. K. C., Fürst, J. J., Frey, H., Gantayat, P., Gillet-Chaulet, F., Girard, C.,  
907 Huss, M., Leclercq, P. W., Linsbauer, A., Machguth, H., Martin, C., Maussion, F., Morlighem, M., Mosbeux, C.,  
908 Pandit, A., Portmann, A., Rabatel, A., Ramsankaran, R., Reerink, T. J., Sanchez, O., Stentoft, P. A., Singh Kumari,  
909 S., van Pelt, W. J. J., Anderson, B., Benham, T., Binder, D., Dowdeswell, J. A., Fischer, A., Helfricht, K., Kutuzov,  
910 S., Lavrentiev, I., McNabb, R., Gudmundsson, G. H., Li, H., and Andreassen, L. M.: How accurate are estimates  
911 of glacier ice thickness? Results from ITMIX, the Ice Thickness Models Intercomparison eXperiment, *Cryosphere*,  
912 11, 949–970, [10.5194/tc-11-949-2017](#), 2017.

913

914 Farinotti, D., Huss, M., Fürst, J. J., Landmann, J., Machguth, H., Maussion, F., and Pandit, A.: A consensus  
915 estimate for the ice thickness distribution of all glaciers on Earth, *Nat. Geosci.*, 12, 168–173, [10.1038/s41561-019-](#)  
916 [0300-3](#), 2019.

917

918 Farinotti, D., Brinkerhoff, D. J., Fürst, J. J., Gantayat, P., Gillet-Chaulet, F., Huss, M., Leclercq, P. W., Maurer, H.,  
919 Morlighem, M., and Pandit, A.: Results from the ice thickness models intercomparison experiment phase 2  
920 (ITMIX2), *Front. Earth Sci.*, 8, 571923, 2021.

921

922 Fischer, A.: Calculation of glacier volume from sparse ice-thickness data, applied to Schaufelferner, Austria, *J.*  
923 *Glaciol.*, 55, 453–460, [10.3189/002214309788816740](#), 2009.



924  
925 Flowers, G. E. and Clarke, G. K. C.: Surface and bed topography of Trapridge Glacier, Yukon Territory, Canada:  
926 digital elevation models and derived hydraulic geometry, *J. Glaciol.*, 45, 165–174, 10.3189/S0022143000003142,  
927 1999.  
928  
929 Frank, T., van Pelt, W. J. J., and Kohler, J.: Reconciling ice dynamics and bed topography with a versatile and fast  
930 ice thickness inversion, *Cryosphere*, 17, 4021–4045, 10.5194/tc-17-4021-2023, 2023.  
931  
932 Frank, T., and van Pelt, W. J. J.: Ice volume and thickness of all Scandinavian glaciers and ice caps, *J. Glaciol.*,  
933 1–34, 10.1017/jog.2024.25, 2024.  
934  
935 Frémand, A. C., Fretwell, P., Bodart, J. A., Pritchard, H. D., Aitken, A., Bamber, J. L., Bell, R., Bianchi, C., Bingham,  
936 R. G., Blankenship, D. D., Casassa, G., Catania, G., Christianson, K., Conway, H., Corr, H. F. J., Cui, X., Damaske,  
937 D., Damm, V., Drews, R., Eagles, G., Eisen, O., Eisermann, H., Ferraccioli, F., Field, E., Forsberg, R., Franke, S.,  
938 Fujita, S., Gim, Y., Goel, V., Gogineni, S. P., Greenbaum, J., Hills, B., Hindmarsh, R. C. A., Hoffman, A. O.,  
939 Holmlund, P., Holschuh, N., Holt, J. W., Horlings, A. N., Humbert, A., Jacobel, R. W., Jansen, D., Jenkins, A., Joket,  
940 W., Jordan, T., King, E., Kohler, J., Krabill, W., Kusk Gillespie, M., Langley, K., Lee, J., Leitchenkov, G., Leuschen,  
941 C., Luyendyk, B., MacGregor, J., MacKie, E., Matsuoka, K., Morlighem, M., Mouginot, J., Nitsche, F. O., Nogi, Y.,  
942 Nost, O. A., Paden, J., Pattyn, F., Popov, S. V., Rignot, E., Rippin, D. M., Rivera, A., Roberts, J., Ross, N., Ruppel,  
943 A., Schroeder, D. M., Siegert, M. J., Smith, A. M., Steinhage, D., Studinger, M., Sun, B., Tabacco, I., Tinto, K.,  
944 Urbini, S., Vaughan, D., Welch, B. C., Wilson, D. S., Young, D. A., and Zirizzotti, A.: Antarctic Bedmap data:  
945 Findable, Accessible, Interoperable, and Reusable (FAIR) sharing of 60 years of ice bed, surface, and thickness  
946 data, *Earth Syst. Sci. Data*, 15, 2695–2710, 10.5194/essd-15-2695-2023, 2023.  
947  
948 Fürst, J. J., Gillet-Chaulet, F., Benham, T. J., Dowdeswell, J. A., Grabiec, M., Navarro, F., Pettersson, R., Moholdt,  
949 G., Nuth, C., and Sass, B.: Application of a two-step approach for mapping ice thickness to various glacier types  
950 on Svalbard, *Cryosphere*, 11, 2003–2032, 2017.  
951  
952 Gärtner-Roer, I., Naegeli, K., Huss, M., Knecht, T., Machguth, H., and Zemp, M.: A database of worldwide glacier  
953 thickness observations, *Glob. Planet. Change.*, 122, 330–344, <https://doi.org/10.1016/j.gloplacha.2014.09.003>,  
954 2014.  
955  
956 Giesen, R. H. and Oerlemans, J.: Response of the ice cap Hardangerjøkulen in southern Norway to the 20th and  
957 21st century climates, *Cryosphere*, 4, 191–213, 10.5194/tc-4-191-2010, 2010.  
958  
959 Gillespie, M. K., Yde, J. C., Andresen, M. S., Citterio, M., and Gillespie, M. A. K.: Ice geometry and thermal regime  
960 of Lyngmarksbræen Ice Cap, West Greenland, *J. Glaciol.*, 1–13, 10.1017/jog.2023.89, 2023.  
961  
962 Gillespie, M. K., Andreassen, L. M., Huss, M., de Villiers, S., Sjørnsen, K. H., Aasen, J., Bakke, J., Cederstrøm, J.  
963 M., Elvehøy, H., Kjølmoen, B., Loe, E., Meland, M., Melvold, K., Nerhus, S. D., Røthe, T. O., Støren, E. W. N.,  
964 Øst, K., and Yde, J. C.: Jostedalbreen ice thickness and bed topography [dataset], 10.58059/yhwr-rx55, 2024.  
965  
966 GlaThiDa Consortium: Glacier Thickness Database 3.1.0, [https://doi.org/World Glacier Monitoring Service, Zurich,  
967 Switzerland](https://doi.org/World%20Glacier%20Monitoring%20Service,%20Zurich,%20Switzerland), 10.5904/wgms-glathida-2020-10, 2020.  
968  
969 Glen, J. W.: The creep of polycrystalline ice, *Proceedings of the Royal Society of London. Series A. Mathematical  
970 and Physical Sciences*, 228, 519–538, 1955.  
971

972 Grab, M., Mattea, E., Bauder, A., Huss, M., Rabenstein, L., Hodel, E., Linsbauer, A., Langhammer, L., Schmid, L.,  
973 and Church, G.: Ice thickness distribution of all Swiss glaciers based on extended ground-penetrating radar data  
974 and glaciological modeling, *J. Glaciol.*, 67, 1074–1092, 2021.

975  
976 [Gudmundsson, G. H.: Transmission of basal variability to a glacier surface, \*J. Geophys. Res.\*, 108, 2253,  
977 10.1029/2002JB002107, 2003.](#)

978  
979 Huss, M. and Farinotti, D.: Distributed ice thickness and volume of all glaciers around the globe, *J. Geophys. Res.*  
980 *Earth Surf.*, 117, 2012.

981  
982 Huss, M. and Farinotti, D.: A high-resolution bedrock map for the Antarctic Peninsula, *Cryosphere*, 8, 1261–1273,  
983 2014.

984  
985 Haakensen, N. and Wold, B.: Breheimen-Stryn: Undersøkelse av bunntopografi på Bødalsbreen, *NVE Rapp.*, 17–  
986 86, 1986.

987  
988 IPCC: *Climate Change 2021: The Physical Science Basis. Contribution of Working Group I to the Sixth Assessment*  
989 *Report of the Intergovernmental Panel on Climate Change*, 2021.

990  
991 Johansson, F. E., Bakke, J., Støren, E. N., Gillespie, M. K., and Laumann, T.: Mapping of the Subglacial  
992 Topography of Folgefonna Ice Cap in Western Norway—Consequences for Ice Retreat Patterns and Hydrological  
993 Changes, *Front. Earth Sci.*, 10, 10.3389/feart.2022.886361, 2022.

994  
995 Kennett M.: Kartlegging av istykkelse og feltavgrensning på Spørteggbreen 1989, *NVE Rapp.* 15-1989,  
996 oppdragsrapport1989\_15.pdf (nve.no), 1989.

997  
998 Kennett M.: Kartlegging av istykkelse og feltavgrensning på Blåmannsisen 1990, *NVE Rapp.* 8-1990  
999 oppdragsrapport1990\_08.pdf (nve.no), 1990.

1000  
1001 Kjøllmoen, B., Andreassen, L.M. and Elvehøy H.: Glaciological investigations in Norway 2023; *NVE Rapp.* xx-2024,  
1002 in prep.

1003  
1004 Lapazarán, J. J., Martín-Español, A., Navarro, F. J., and Otero, J.: On the errors involved in ice-thickness estimates  
1005 I: ground-penetrating radar measurement errors, *J. Glaciol.*, 62, 1008–1020, 10.1017/jog.2016.93, 2016.

1006  
1007 Laumann, T. and Nesje, A.: The impact of climate change on future frontal variations of Briksdalsbreen, western  
1008 Norway, *J. Glaciol.*, 55, 789–796, 10.3189/002214309790152366, 2009.

1009  
1010 Laumann, T. and Nesje, A.: Spørteggbreen, western Norway, in the past, present and future: Simulations with a  
1011 two-dimensional dynamical glacier model, *Holocene*, 24, 842–852, 10.1177/0959683614530446, 2014.

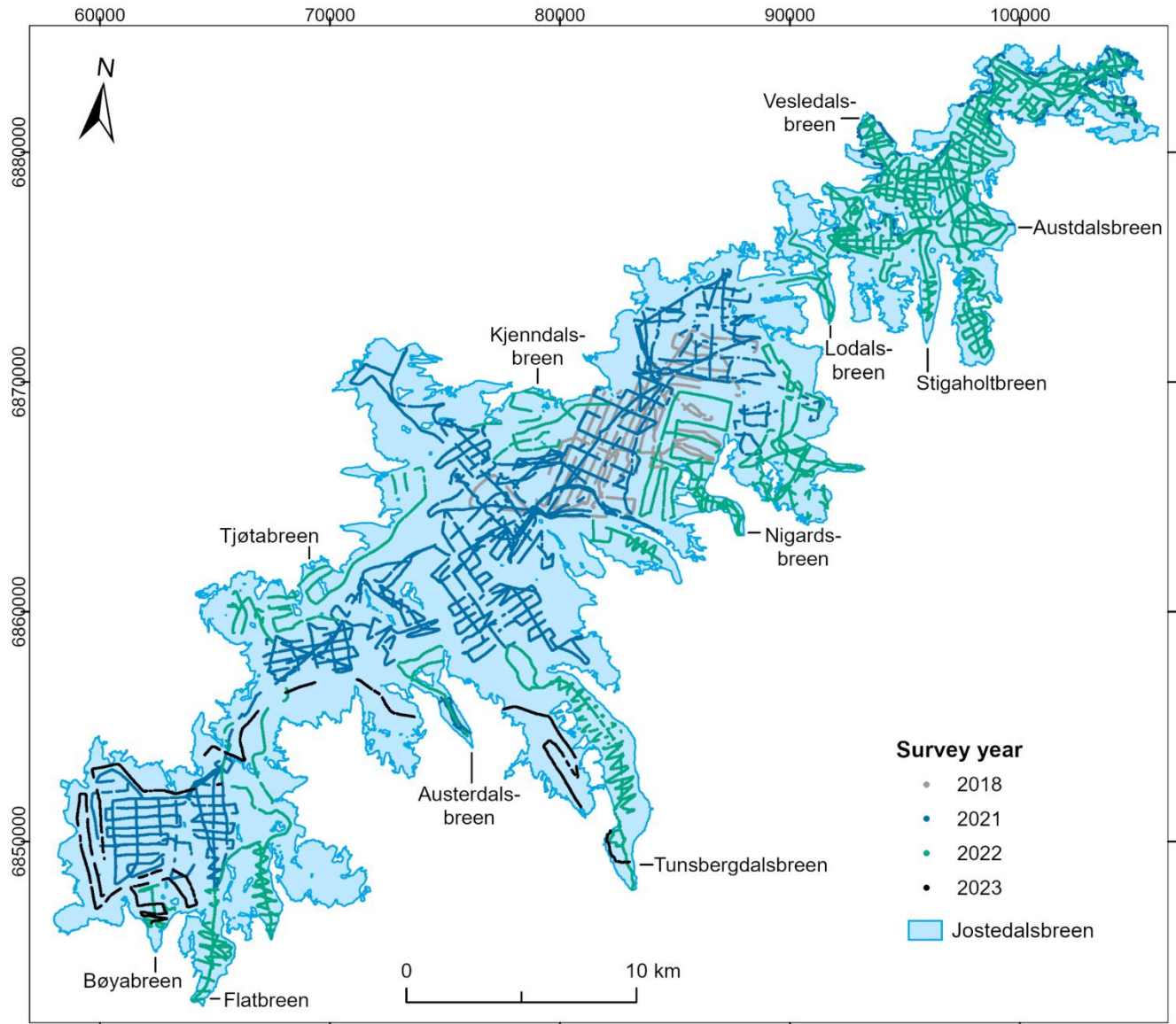
1012  
1013 Lindbäck, K., Kohler, J., Pettersson, R., Nuth, C., Langley, K., Messerli, A., Vallot, D., Matsuoka, K., and Brandt,  
1014 O.: Subglacial topography, ice thickness, and bathymetry of Kongsfjorden, northwestern Svalbard, *Earth Syst. Sci.*  
1015 *Data*, 10, 1769–1781, 10.5194/essd-10-1769-2018, 2018.

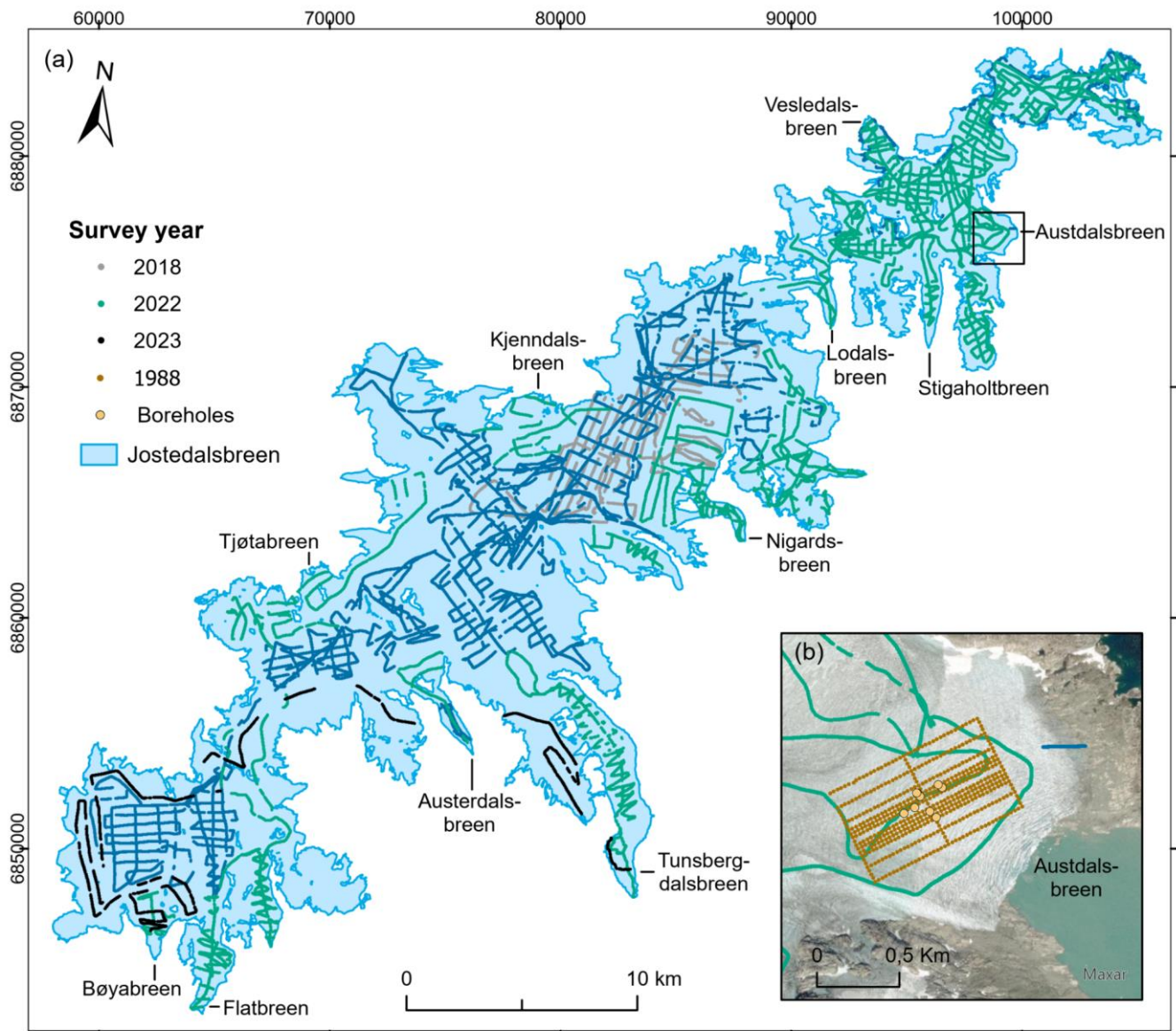
1016  
1017 Linsbauer, A., Paul, F., and Haeberli, W.: Modeling glacier thickness distribution and bed topography over entire  
1018 mountain ranges with GlabTop: Application of a fast and robust approach, *J. Geophys. Res. Earth Surf.*, 117, 2012.

1019  
1020 Millan, R., Mouginot, J., Rabatel, A., and Morlighem, M.: Ice velocity and thickness of the world's glaciers, *Nat.*  
1021 *Geosci.*, 15, 124–129, 10.1038/s41561-021-00885-z, 2022.

1022 Mingo, L. and Flowers, G. E.: An integrated lightweight ice-penetrating radar system, *J. Glaciol.*, 56, 709–714,  
1023 10.3189/002214310793146179, 2010.  
1024  
1025  
1026 Morlighem, M., Williams, C. N., Rignot, E., An, L., Arndt, J. E., Bamber, J. L., Catania, G., Chauché, N., Dowdeswell,  
1027 J. A., Dorschel, B., Fenty, I., Hogan, K., Howat, I., Hubbard, A., Jakobsson, M., Jordan, T. M., Kjeldsen, K. K.,  
1028 Millan, R., Mayer, L., Mouginot, J., Noël, B. P. Y., O’Cofaigh, C., Palmer, S., Rysgaard, S., Seroussi, H., Siegert,  
1029 M. J., Slabon, P., Straneo, F., van den Broeke, M. R., Weinrebe, W., Wood, M. and Zinglensen, K. B.: BedMachine  
1030 v3: Complete bed topography and ocean bathymetry mapping of Greenland from multibeam echo sounding  
1031 combined with mass conservation, *Geophys. Res. Lett.*, 44, 11,051–11,061. 10.1002/2017GL074954, 2017.  
1032  
1033 Navarro, F. and Eisen, O.: Ground-penetrating radar in glaciological applications, in: Remote sensing of glaciers:  
1034 Techniques for topographic, spatial and thematic mapping of glaciers, Taylor & Francis London, 195–229, 2009.  
1035  
1036 Nesje, A., Johannessen, T., and Birks, H. J. B.: Briksdalsbreen, western Norway: climatic effects on the terminal  
1037 response of a temperate glacier between AD 1901 and 1994, *Holocene*, 5, 343–347,  
1038 10.1177/095968369500500310, 1995.  
1039  
1040 Ogier, C., van Manen, D.-J., Maurer, H., Räss, L., Hertrich, M., Bauder, A., and Farinotti, D.: Ground penetrating  
1041 radar in temperate ice: englacial water inclusions as limiting factor for data interpretation, *J. Glaciol.*, 1–12, 2023.  
1042  
1043 [Paul F., Andreassen L.M., and Winsvold S.H.: A new glacier inventory for the Jostedalbreen region, Norway, from  
1044 Landsat TM scenes of 2006 and changes since 1966, \*Ann. Glaciol.\*, 52, 153-162, 10.3189/172756411799096169,  
1045 2011.](#)  
1046  
1047 Pettersson, R., Christoffersen, P., Dowdeswell, J. A., Pohjola, V. A., Hubbard, A., and Strozzi, T.: Ice thickness  
1048 and basal conditions of Vestfonna ice cap, eastern Svalbard, *Geogr. Ann. A: Phys. Geogr.*, 93, 311–322, 2011.  
1049  
1050 Plewes, L. A. and Hubbard, B.: A review of the use of radio-echo sounding in glaciology, *Prog. Phys. Geogr.*, 25,  
1051 203–236, 2001.  
1052  
1053 Rounce, D. R., Hock, R., Maussion, F., Hugonnet, R., Kochtitzky, W., Huss, M., Berthier, E., Brinkerhoff, D.,  
1054 Compagno, L., and Copland, L.: Global glacier change in the 21st century: Every increase in temperature matters,  
1055 *Science*, 379, 78–83, 2023.  
1056  
1057 Schlegel, R., Kulesa, B., Murray, T., and Eisen, O.: Towards a common terminology in radioglaciology, *Ann.*  
1058 *Glaciol.*, 63, 8–12, 2022.  
1059  
1060 Seier, G., Abermann, J., Andreassen, L. M., Carrivick, J. L., Kielland, P. H., Löffler, K., Nesje, A., Robson, B. A.,  
1061 Røthe, T. O., Scheiber, T., Winkler, S. and Yde, J. C.: Glacier thinning, recession and advance, and the associated  
1062 evolution of a glacial lake between 1966 and 2021 at Austerdalsbreen, western Norway, *Land. Degrad. Dev.*, 2024.  
1063  
1064 Sellevold, M. and Kloster, K.: Seismic measurements on the glacier Hardangerjøkulen, Western Norway, *Nor.*  
1065 *Polarinst. Årb.*, 87–91, 1964.  
1066  
1067 Smith, B. E. and Evans, S.: Radio echo sounding: absorption and scattering by water inclusion and ice lenses, *J.*  
1068 *Glaciol.*, 11, 133–146, 1972.  
1069  
1070 Sverrisson, M., Jóhannesson, Æ., and Björnsson, H.: Instruments and Methods: Radio-Echo Equipment for Depth  
1071 Sounding of Temperate Glaciers, *J. Glaciol.*, 25, 477–486, 1980.

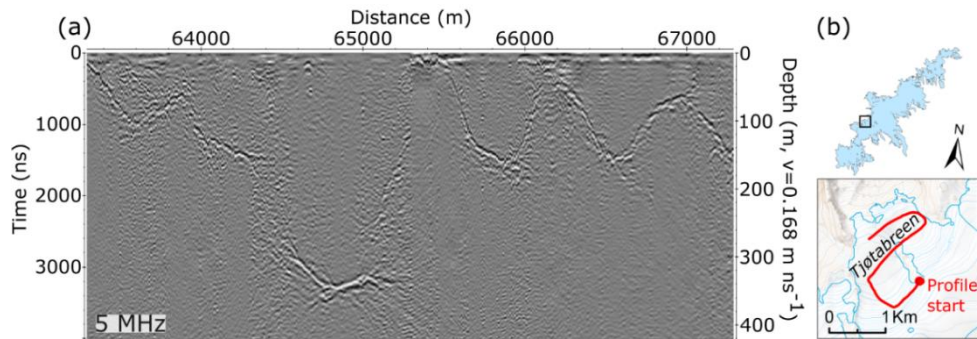
1072  
1073 Sætrang, A. C.: Istykkelsesmålinger med breradar på Austdalsbreen, Heli-Anlegg Rapp., 5–88, 1988.  
1074  
1075 Sætrang, A. C. and Holmqvist, E.: Kartlegging av istykkelse på nordre Jostedalsbreen, NVE Rapp., 8-1987, 1987.  
1076  
1077 Sætrang, A. C. and Wold, B.: Results from the radio echo-sounding on parts of the Jostedalsbreen ice cap, Norway,  
1078 Ann. Glaciol., 8, 156–158, 1986.  
1079  
1080 Terratec: Laserskanning for nasjonal detaljert høydemodell, NDH Jostedalsbreen 2pkt, 2020.  
1081  
1082 Welty, E., Zemp, M., Navarro, F., Huss, M., Fürst, J. J., Gärtner-Roer, I., Landmann, J., Machguth, H., Naegeli, K.,  
1083 and Andreassen, L. M.: Worldwide version-controlled database of glacier thickness observations, Earth Syst. Sci.  
1084 Data., 12, 3039–3055, 2020.  
1085  
1086 Yde, J. C., Gillespie, M. K., Løland, R., Ruud, H., Mernild, S. H., Villiers, S. D., Knudsen, N. T., and Malmros, J. K.:  
1087 Volume measurements of Mittivakkat Gletscher, southeast Greenland, J. Glaciol., 60, 1199–1207, 2014.  
1088  
1089 Østrem, G., Liestøl, O., and Wold, B.: Glaciological investigations at Nigardsbreen, Norway, Nor. Geogr. Tidsskr.,  
1090 30, 187–209, 10.1080/00291957608552005, 1976.  
1091  
1092 Åkesson, H., Nisancioglu, K. H., Giesen, R. H., and Morlighem, M.: Simulating the evolution of Hardangerjøkulen  
1093 ice cap in southern Norway since the mid-Holocene and its sensitivity to climate change, Cryosphere, 11, 281–  
1094 302, 2017.  
1095  
1096





1101  
1102 **Figure A1: (a) Locations of ice thickness measurements divided into survey year- and (b) ice thickness measurements**  
1103 **on Austdalsbreen, including the locations of the 1988 survey lines and boreholes from 1986 and 1987. The coordinate**  
1104 **system on both maps is UTM 33N, datum ETRS89. The background imagery in (b) is from Esri**  
1105 **([https://services.arcgisonline.com/ArcGIS/rest/services/World\\_Imagery/MapServer](https://services.arcgisonline.com/ArcGIS/rest/services/World_Imagery/MapServer)) and in this area relies on a Maxar**  
1106 **mosaic with images from 2019 and 2021.**

1108 **Appendix B**



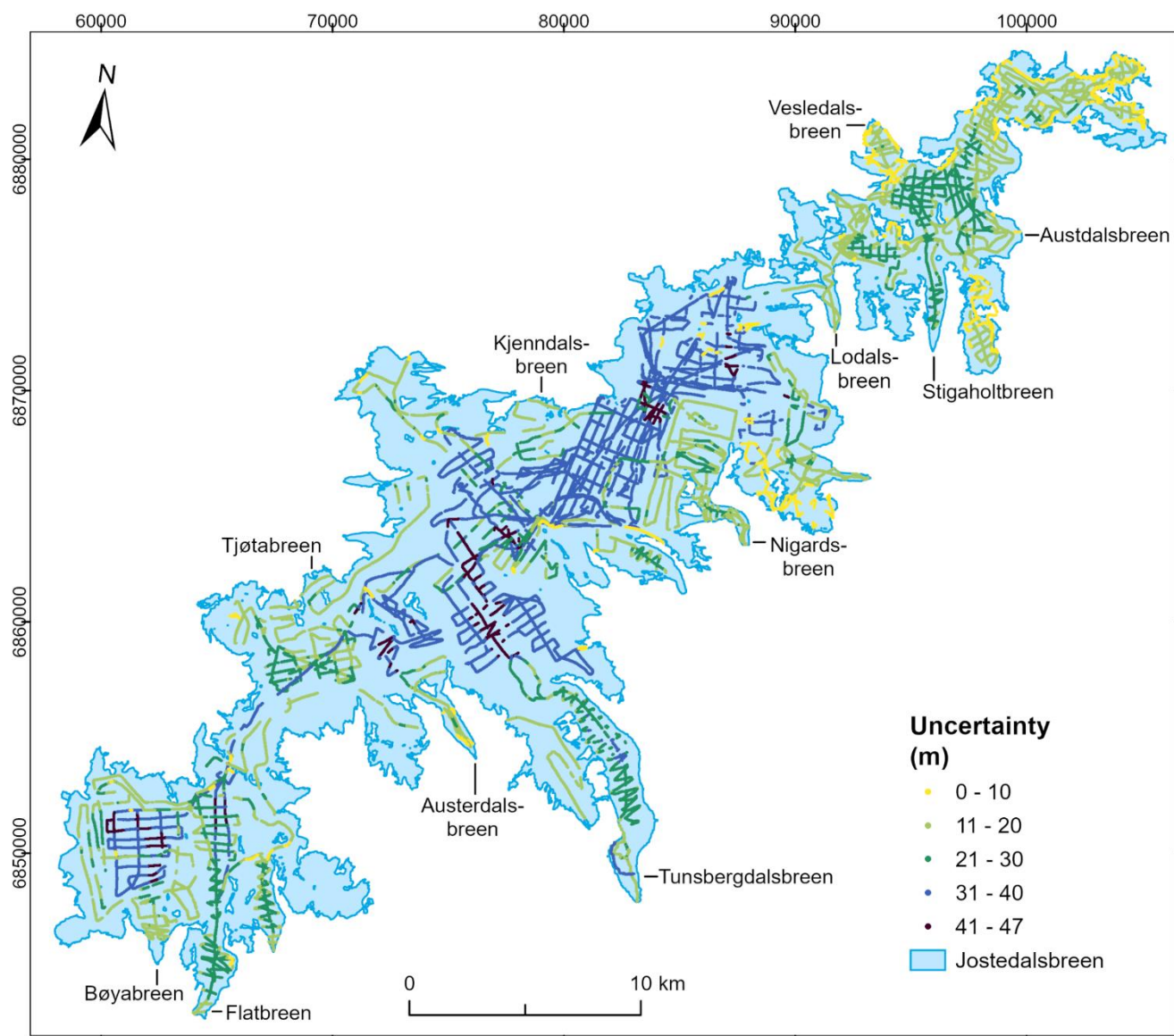
1111

1112 **Figure B1:** (a) Example of measurements with the 5 MHz airborne radar system. (b) The profile was located along a

1113 transect at Tjøtabreen (Fig. 1). The background map in (b) is from the Norwegian Mapping Authority (WMS for

1114 Topografisk Norgeskart available at <https://www.geonorge.no/>) and the 2019 glacier outlines are from Andreassen et

1115 al. (2022).



1119

1120

1121

**Figure B4-C1:** Total measurement uncertainty associated with each ice thickness observation calculated using the method described by Lapazaran et al. (2016). The coordinate system is UTM 33N, datum ETRS89.